Biophysical Journal
Article

Biophysical Society

Dynamics of PAR Proteins Explain the Oscillation and Ratcheting Mechanisms in Dorsal Closure

Clinton H. Durney,[1] Tony J. C. Harris,[2] and James J. Feng[1,3,*]
[1]Department of Mathematics, University of British Columbia, Vancouver, British Columbia, Canada; [2]Department of Cell & Systems Biology, University of Toronto, Toronto, Ontario, Canada; and [3]Department of Chemical and Biological Engineering, University of British Columbia, Vancouver, British Columbia, Canada

ABSTRACT We present a vertex-based model for *Drosophila* dorsal closure that predicts the mechanics of cell oscillation and contraction from the dynamics of the PAR proteins. Based on experimental observations of how aPKC, Par-6, and Bazooka translocate from the circumference of the apical surface to the medial domain, and how they interact with each other and ultimately regulate the apicomedial actomyosin, we formulate a system of differential equations that captures the key features of dorsal closure, including distinctive behaviors in its early, slow, and fast phases. The oscillation in cell area in the early phase of dorsal closure results from an intracellular negative feedback loop that involves myosin, an actomyosin regulator, aPKC, and Bazooka. In the slow phase, gradual sequestration of apicomedial aPKC by Bazooka clusters causes incomplete disassembly of the actomyosin network over each cycle of oscillation, thus producing a so-called ratchet. The fast phase of rapid cell and tissue contraction arises when medial myosin, no longer antagonized by aPKC, builds up in time and produces sustained contraction. Thus, a minimal set of rules governing the dynamics of the PAR proteins, extracted from experimental observations, can account for all major mechanical outcomes of dorsal closure, including the transitions between its three distinct phases.

INTRODUCTION

Dorsal closure (DC) is an important morphogenetic process during the embryonic development of *Drosophila*. During DC, two flanking epidermal tissues are fused together to close an opening on the dorsal side of the embryo, covering up the thin amnioserosa (AS) tissue. The entire DC process, lasting ~3.5 h, exhibits three distinct phases, showing great spatial and temporal coordination. The early phase is characterized by AS cell oscillations and no loss in overall tissue area. The ensuing slow phase exhibits a gradual loss in overall tissue area and a dampening of cellular oscillations. Finally, the fast phase displays rapid and persistent loss of tissue area and cessation of the oscillations. Although recent experiments have identified several contributing factors in DC (1–6), the connections between them remain elusive.

For the early phase, the key question is the cause of the cyclic oscillation of the cell area. On the apical surface, a medial network of actomyosin periodically assembles and disassembles with a period of ~4 min (1,7–9). The cell contracts after the assembly of the actomyosin network and relaxes when the network disassembles (7,10). After each cycle, the cell area returns to more or less the previous state. The contraction of one cell pulls on its neighbors, yielding a preference for antiphase pulsing between neighboring cells (1). But Blanchard et al. (4) have also observed transient "ribbons" of cells that are simultaneously contracting or expanding. It remains to be ascertained whether the oscillatory behavior originates from the autonomous dynamics within each cell or from the communications between neighbors or even both (1,11,12).

Naturally, one seeks an explanation for the oscillatory behavior from biochemical signaling (7,13–16). David et al. (7) highlighted the roles of the PAR proteins. Bazooka (Baz) promotes the duration of actomyosin contraction, whereas the Par-6/aPKC complex promotes the lull time between contractions. More recently, David et al. (15) further delineated the spatial and temporal relationship among the PAR proteins and the actomyosin network that periodically assembles in the apicomedial domain of the AS cells. The actomyosin recruits aPKC from the circumference of the apical surface toward the medial region, where it forms puncta that colocalize with the actomyosin network. In turn, aPKC recruits Baz into the medial region. Because aPKC is known to phosphorylate and inhibit myosin (17,18) and cause apical relaxation in AS cells (7)—whereas Baz promotes apical constriction through complexing aPKC

Submitted June 4, 2018, and accepted for publication October 16, 2018.
*Correspondence: james.feng@ubc.ca
Editor: Ana-Suncana Smith.
https://doi.org/10.1016/j.bpj.2018.10.014

(7)—David et al. (15) hypothesized that the PAR proteins form a negative feedback loop with the medial actomyosin network to produce the oscillatory outcome. The expansion phase of the oscillation may be driven by the elasticity of the AS cells and the contraction of neighboring cells.

To rationalize the areal contraction of the slow phase, the two central ideas are the ratcheting mechanism and the supracellular actin cable, although recent evidence has also suggested cell volume loss as a contributor (19). The concept of an intracellular or internal ratchet was introduced by Martin et al. (10,20) to explain the pulsed constriction of *Drosophila* ventral furrow cells. After each contraction, a cell is prevented from returning to its prior apical area by tension emanating from an apicomedial actomyosin meshwork, which stabilizes the cell shape and produces net constriction. Consistent with the above, the live images of David et al. (7,15) demonstrate an apicomedial actomyosin network that grows stronger over each pulse in the slow phase, a transition that coincides with greater aPKC-Baz interaction in the medial domain. Roughly concurrent with the onset of the slow phase, an actin cable appears along the boundary between the AS tissue and the surrounding epidermis. It encircles the AS like a purse string and clamps down on the tissue. This was initially considered the main cause of AS contraction (1,21), but more recent work has challenged its importance (9,20,22–24). For example, Wells et al. (9) disrupted the purse string by severing one or both of the canthi and observed that closure proceeded normally. Pasakarnis et al. (23) used selective force elimination to demonstrate that the AS cells alone are capable of driving DC. Ducuing and Vincent (24) reported that the actin cable does not contribute appreciably to the dorsal-ward movement of the leading edges. Thus, a consensus seems to be forming on a secondary role for the actin cable.

The advent of the fast phase brings a few new factors. As the AS tissue narrows, the opposing epidermis extends filopodia onto the opposite side, which then pull to help the closure (25–27). This is known as zippering. Much like the actin cable, the zippering forces have been shown to be superfluous for complete closure (9). Moreover, AS cell apoptosis contributes to rapid closure by dropping out of the plane of the AS, effectively reducing the tissue area (3,8,21,28). Finally, the epidermis may elongate actively to assist rapid closure in the fast phase (29).

Mathematical modeling has been used to integrate the experimental insights above into a more precise and quantitative understanding (26,30,31). A majority of these models are purely mechanical, imposing prescribed forces on the tissue (32) or on individual cells (1,33) and examining their elastic or viscoelastic responses (34,35). In such models, the cellular oscillations of the early phase are the result of an externally imposed force or the mechanical coupling between cells (1,32). More recent work strove to integrate the mechanical and biochemical aspects of the process (36,37). Wang et al. (22) assumed a simple kinetic equation for a hypothetical signaling molecule and predicted cyclic myosin dynamics for the early phase from a negative feedback loop. By an ad hoc device of shrinking the resting length of the elastic cell borders, their model produced a net loss of cell and tissue area. Similarly, Machado et al. (11) relied on a feedback loop between a putative signaling molecule and actin turnover, which was a proxy for myosin attachment and detachment. This model showed how the rate of actin turnover may modulate the period of AS cell oscillation. These models are commendable in seeking a deeper explanation of the DC dynamics from the chemical-mechanical coupling, but they have incorporated much phenomenology and left several fundamental questions unanswered. What is the mechanism for the spontaneous oscillation in the early phase? What mechanism organizes the ratcheting behavior in the early phase? What triggers the transition from one phase to the next?

These questions have motivated our model, which integrates earlier vertex models (1,22) with the biochemical insights of recent experiments (7,15) to provide a comprehensive picture of DC. In particular, we will demonstrate how the PAR proteins interact with a regulator of the actomyosin network to produce not only the oscillation in the early phase but also the ratcheting in the slow phase and the persistent contraction in the fast phase. Essentially all features of the DC process, except for apoptosis of AS cells and zippering that affect the final closure, can be explained by a cell-mechanical framework supplied with a few experimental observations regarding the movement and biochemistry of the PAR proteins.

MODEL FORMULATION

We represent the AS tissue by a two-dimensional vertex model of 121 hexagonal cells (Fig. 1 *a*). Because the AS cells are thin and squamous, and the actomyosin and signaling proteins of interest are localized to the apical surface, we adopt a two-dimensional planar representation (22). Each cell has six peripheral nodes connected by passively elastic edges due to the the actin cortex. A central node is connected to the circumference by elastic spokes that also have an active force component because of myosin contraction (Fig. 1 *a*, *inset*). The AS is flanked by an epidermis that resists DC (21,38) but can also engage in active elongation (29). As a simplified treatment, we surround the AS by elastic tension lines (*blue lines* in Fig. 1 *a*) attached to an outer boundary that is fixed in space.

The mechanical model essentially follows the previous work of Wang et al. (22), and more details can be found in Supporting Materials and Methods, Section S1. In brief, each cell edge or spoke carries a linearly elastic force depending on the elongation or compression of that segment relative to its rest length. Each spoke also carries an active myosin force proportional to the number of myosin motors on it (Eq. S3), which is in turn determined by the

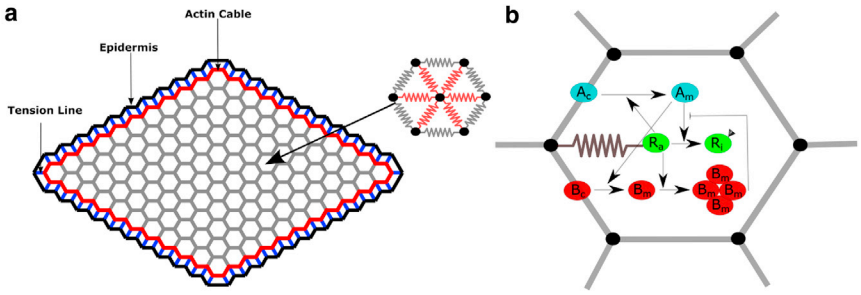

FIGURE 1 (*a*) The AS tissue comprises 121 hexagonal cells, and the big arrow points to a "representative cell" whose dynamics are reported later in the study. Each cell has six edges and six spokes. The edges and spokes are passively elastic represented by springs, and the spokes also carry an active myosin force. The AS tissue is linked by elastic tension lines to a stationary epidermis, and the border of the AS tissue represents the supracellular actin cable. (*b*) The translocation and interactions of the PAR proteins inside each cell. Apicomedial actomyosin, represented by its regulator R_a, recruits apico-circumferential aPKC ($A_c \rightarrow A_m$) medially to form a pool of apicomedial aPKC, which phosphorylates the active regulator R_a into an inactive form R_i. Concomitantly, A_m recruits its own inhibitor Baz medially ($B_c \rightarrow B_m$), which in a clustered form sequesters A_m. R_a promotes the clustering of B_m. To see this figure in color, go online.

actomyosin regulator to be discussed in the kinetic model below (Eq. S1). Each central or peripheral node executes overdamped motion according to the vector sum of all the edge and spoke forces acting on it (Eq. S4). The supracellular actin cable surrounding the AS tissue is modeled by a contractile force that varies piecewise linearly in time (Eq. S5); the time of onset and duration of linear increase before leveling off are fitted to experimental data. The tension lines connecting the AS to the surroundings are linearly elastic, with a force that balances the AS tissue tension in an average sense. Finally, we neglect zippering forces in our model.

Our kinetic model is, to our knowledge, novel in its detailed treatment of the molecular signaling pathways, based on observations of the transport and interaction of the PAR proteins (7,15,39), the identity of the target protein for aPKC (17,40–42), and the clustering dynamics of apicomedial Baz (43–45). Fig. 1 *b* depicts the protein species tracked in our model as well as their spatial localization and interactions. The PAR proteins—Baz, Par-6, and aPKC—have been known to regulate the apicomedial localization and activation of actomyosin in AS (7,15). Of the three, Par-6 always acts in conjunction with aPKC (7,46), and we will consider the aPKC-Par-6 complex a single entity in the following, referring to it simply as aPKC. Although aPKC has long been known to inhibit actomyosin, its target, which is presumably a regulator or effector of RhoA/Rho1, has not been unequivocally identified. In mammalian cells, Smurf1 can be phosphorylated by aPKC to cause RhoA degradation (17), and aPKC may also act through p190RhoGAP to inhibit RhoA (40). More recent evidence points to Rho kinase (Rok) as a likely target because phosphorylation by aPKC causes Rok to dissociate from the cell cortex (41). In the *Drosophila* placode border, aPKC phosphorylates Rok to deactivate its role in recruiting myosin (42). Based on these, Rok is a strong candidate for the myosin regulator during DC. To be prudent, however, we will use a generic name Reg in the model.

Another important feature of Fig. 1 *b* is the localization and translocation of aPKC and Baz. At the onset of DC, the kinase-active store of aPKC is mostly bound to the plasma membrane to either of the two membrane proteins Cdc42 or Crumbs (47). Because aPKC is prevented from accumulating on the basolateral plasma membranes by a molecular exclusion mechanism (47), it has been observed mostly on the apical surface and concentrated along the circumference (7,15). Meanwhile, Baz is also concentrated in the adherens junctions in the apico-circumference region (47). During DC, the circumferential aPKC and Baz are progressively recruited to the apicomedial domain (15). More specifically, aPKC is recruited by the actomyosin network, and it, in turn, recruits Baz. Both proteins form puncta in the apicomedial region of the cell. Schematically, Fig. 1 *b* uses two arrows to represent these two successive recruitments:

$$\begin{aligned} A_c &\xrightarrow[R_a]{k_1} A_m(\text{Translocation with delay } \tau) \\ B_c &\xrightarrow[A_m]{k_2} B_m(\text{Translocation and phosphorylation}) \end{aligned},$$

where we indicate both the rate constant and the recruiting agent for each migration. The exact mechanisms of the circumference-to-apicomedial translocation are unknown at present, although several possibilities—e.g., diffusion through the cytosol, direct translocation of large protein complexes along the membrane, and actomyosin advection—have been suggested based on *Caenorhabditis elegans* data (43–45). To account for the multiple steps involved in this process that are not explicitly modeled, we introduce a time delay τ in converting the circumferential aPKC A_c to the medial aPKC A_m. For the transport of Baz, on the other hand, we do not implement an explicit delay. As explained below, B_m undergoes an oligomerization into a clustered form before its interaction with A_m. This two-step process will be modeled explicitly, with kinetic rates that amount to an effective delay that allows A_m the time to inactivate R_a. Besides, the Baz clusters have such a high capacity of sequestering aPKC that only a small fraction of B_c will have translocated medially (Fig. S8 *b*). Thus, a further delay matters little to the model prediction. This is confirmed by numerical tests (Fig. S9).

Once medial, the PAR proteins undergo a series of dynamic interactions that eventually leads to the cyclic

assembly and disassembly of the medial actomyosin network in each AS cell. Medial aPKC inhibits actomyosin contraction by binding with an active form of Reg (R_a), followed by a phosphorylation event and a quick unbinding, yielding an inactive form of Reg (R_i) and the original aPKC molecule (41,42):

$$\begin{array}{l} A_m + R_a \xrightarrow{k_3} AR \xrightarrow{k_4} A_m + R_i (\text{Reg phosphorylation}) \\ \varnothing \xrightarrow{q_R} R_a (\text{Reg production}) \end{array}.$$

We neglect specific reactivation of the inactive form of Reg (R_i) into the active form R_a and instead account for such reactivation through a Reg source q_R. This is motivated on the one hand by observations that an expression of upstream actomyosin regulators—e.g., DRhoGEF2 acting on Rho1 for downstream activation of Rok or Diaphanous (16)—is necessary to maintain wild-type AS cell behavior. On the other hand, q_R also enables the model to predict a rising level of apicomedial myosin in later stages of DC, which is a prominent feature in vivo both at the protein level (7,15) and at the level of induced gene expression in the tissue (48).

The apicomedial Baz molecules (B_m) become clustered (B_m^*) under the influence of R_a. Imaging evidence suggests that this occurs through the mechanical tension produced by the actomyosin networks rather than chemical binding to the actomyosin; the tension may enhance Baz oligomerization through structural reorganization of the multidomain protein (43,49). The Baz clusters B_m^* then sequester A_m and antagonize its effect on myosin regulation (15,43–45):

$$\begin{array}{l} B_m \underset{k_6}{\overset{k_5(R_a)}{\rightleftharpoons}} B_m^* (\text{Baz clustering}) \\ A_m + B_m^* \underset{k_8}{\overset{k_7}{\rightleftarrows}} AB (\text{aPKC} - \text{Baz complex with aPKC sequestration}). \end{array}$$

These reactions are indicated, respectively, by pointed and blunted arrows in Fig. 1 *b*. The sequestration of aPKC by Baz clusters has an uncertain stoichiometry. It is known that each Baz protein has multiple binding sites for the Par-6-aPKC complex (15,50). Depending on the number of Baz in the cluster, each cluster can potentially sequester a large number of aPKC molecules before it is saturated. For lack of quantitative knowledge of the stoichiometry, we have made the simplifying assumption that a Baz cluster, once formed, can continue to sequester aPKC without being saturated. As will be seen later, this affects the model only in one minor aspect: the consumption of Baz in the medial domain.

The interactions described above establish a competition for A_m by R_a and B_m^* and a potential scheme for generating a delayed negative feedback loop as hypothesized by David et al. (15). On reaching the apicomedial domain, A_m antagonizes R_a and causes the actomyosin network to disassemble. But A_m also recruits B_m to the medial domain, where B_m clusters into an agent that inhibits A_m, giving R_a the time to accumulate and reassemble the actomyosin network. The inhibition of A_m by B_m^* is helped by the fact that the dissociation rates k_6 for B_m^* and k_8 for AB are both slow, making B_m^* a potent aPKC sequestration mechanism (43–45). The transport and kinetic processes can be described by the following coupled differential equations, all protein species being expressed in terms of concentration:

$$\frac{dA_c}{dt} = -k_1 A_c R_a, \tag{1}$$

$$\frac{dB_c}{dt} = -k_2 A_m B_c, \tag{2}$$

$$\frac{dA_m}{dt} = k_1 A_c(t-\tau) R_a(t-\tau) - k_3 A_m R_a + k_4 AR - k_7 A_m B_m^* + k_8 AB, \tag{3}$$

$$\frac{dB_m}{dt} = k_2 A_m B_c - k_5 B_m R_a + k_6 B_m^*, \tag{4}$$

$$\frac{dR_a}{dt} = q_R - k_3 A_m R_a, \tag{5}$$

$$\frac{dAR}{dt} = k_3 A_m R_a - k_4 AR, \tag{6}$$

$$\frac{dR_i}{dt} = k_4 AR, \tag{7}$$

$$\frac{dB_m^*}{dt} = k_5 B_m R_a - k_6 B_m^*, \tag{8}$$

and

$$\frac{dAB}{dt} = k_7 A_m B_m^* - k_8 AB. \tag{9}$$

The regulator R_a serves as the link between the kinetics of the biochemistry and the mechanics of actomyosin contraction. The scheme of distributing R_a in each cell among the six spokes and the kinetic equation for the attachment and detachment of myosin motors are the same as in Wang et al. (22), and details are given in the Supporting Materials and Methods, Section S1. The model has a number of parameters, which are evaluated from experimental data when possible. To address uncertainties in the parameter values, we have performed a sensitivity analysis and found the kinetic model to be robust around the chosen values. Details of this analysis, along with a table of the parameter values, can be found in the Supporting Materials and Methods, Section S2.

We start the simulation with an initial circumferential aPKC store of A_c and Baz store of B_c and no Reg or myosin in the medial region. In the real AS, the cells exhibit phase lags among the neighbors, and they oscillate preferentially in antiphase (1). To introduce the phase lag, we stagger the start of the kinetic model among the cells by a time randomly chosen between $t = 0$ and $t = T$, where $T \sim 260$ s is the period of oscillations observed in experiments (1) and also captured by our simulation.

RESULTS

Our model is able to predict the three distinct phases of DC. Fig. 2 depicts the temporal evolution of the area of a representative cell in Fig. 2 *a* and that of the whole tissue in Fig. 2 *b*. The early phase features an oscillating tissue area without a sustained decrease over the cycles. This gives way to the slow phase, which starts with the onset of net tissue area loss and ends with the cessation of oscillation on the cell level. The total loss in tissue area amounts to about 18% during the slow phase. Finally, the fast phase is distinguished by a mostly monotonic shrinking of the cell area and a rapid contraction of the tissue area toward closure. The dynamics of the entire process can be viewed in Video S1. In the following, we explore the molecular mechanisms that underlie each phase and trigger the transition from one to the next.

Early phase: oscillations

The purpose of this subsection is to investigate the origin of the oscillatory behavior of the AS cells within the context of the chemical signaling pathways detailed in the kinetic model. Fig. 3 shows the early-phase dynamics of the myosin motors and the cell area of the representative cell highlighted in Fig. 1 *a*. For this cell, the PAR protein kinetics begin at $t = 179$ s, before which the cell is only subject to mechanical forces from its neighbors, which cause the initial increase in its area. Once the biochemical network is activated, cell behavior becomes dominated by the internal myosin dynamics (see discussion of Fig. S6 in Supporting Materials and Methods, Section S3). Persistent oscillations of the cell area and the myosin level develop in time. The mean period of oscillations, $T \approx 260$ s, matches experimental observations (1,4). Parametric studies show that T is not very sensitive to the kinetic rate parameters (Figs. S1 and S2), but it increases with τ (Fig. S3). Within the context of the model, this suggests that the period of oscillations is an outcome of the transport and activation mechanisms of apicomedial aPKC. Moreover, the cell area oscillates roughly in antiphase with the myosin, with an amplitude of about 20% among AS cells (Fig. 3). The maximum of myosin precedes the minimum of the cell area slightly, in agreement with experimental observations (4,7,22). The delay in the cell contraction is due to viscous damping. We have also calculated the cross correlation of the area change between neighboring cells. Although the cells have been given a random initial phase lag, once they settle into a regular oscillation, the mechanical coupling among neighbors produces on average a negative correlation (Fig. S6 *a*), again in agreement with experimental observations (1,4).

The area of the entire tissue also exhibits temporal variations (Fig. 2 *b*; Video S1), but the overall change is less than 6% during the early phase. As the actomyosin network is activated throughout the AS cells, the tissue area first declines by about 5% and then recovers to roughly its initial area. The decline is owing to the fact that the first few cycles of myosin oscillation are particularly strong, with large amplitudes (see Fig. 4 *a* below). In time, it settles into a milder oscillatory pattern, producing the recovery in tissue area. This process manifests itself in the evolution of individual cell areas by a decrease in the amplitude of the area (Fig. 2 *a*). One can also discern small-amplitude oscillations in the whole tissue area, a collective effect of the oscillation of all the AS cells. In addition, we see little difference in behavior between the leading-edge cells and those in the interior (Fig. S10).

Under the assumptions of the model, the origin of the oscillation can be sought from the temporal and spatial relationship among the PAR proteins and the regulator. The direct cause for the myosin pulse is a pulse in R_a (Fig. 4 *a*). R_a grows because of the steady production q_R (Eq. 5), and its growth recruits A_m with a delay τ (Eq. 3).

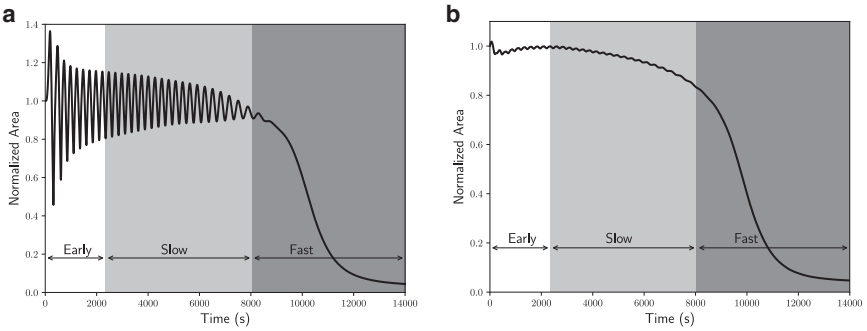

FIGURE 2 The temporal evolution of (*a*) the area of the representative cell of Fig. 1 and (*b*) the entire tissue area. Both areas are normalized by their initial values. The early phase shows oscillatory behavior, the slow phase shows dampening oscillations and gradual area loss, and the fast phase shows persistent loss of area.

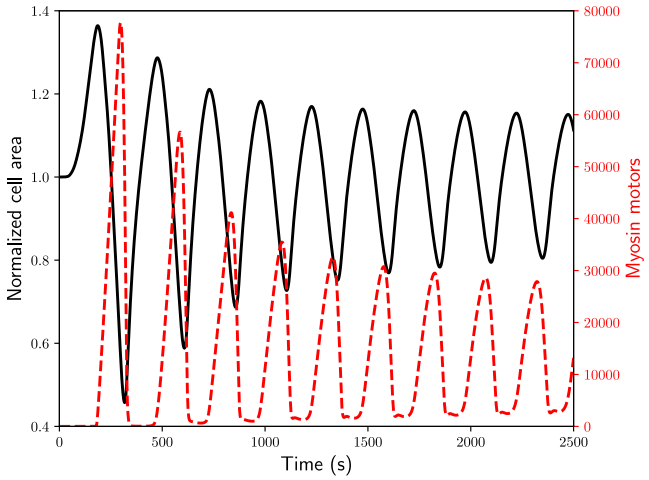

FIGURE 3 Early phase dynamics of the normalized area of the representative cell (*black solid line*) and the total myosin inside the cell (*red dashed line*). To see this figure in color, go online.

As A_m accumulates in the apicomedial domain, it continues to phosphorylate and deactivate R_a, causing the latter to peak and then sharply decline (Fig. 4 *b*). Thus, the medial myosin network disassembles as a result of the medial aPKC (7). Meanwhile, A_m recruits Baz (Eq. 4) so B_m rises in tandem with A_m (Fig. 4 *c*). As B_m oligomerizes into B_m^* (Fig. 4 *d*), the latter grows and in turn sequesters A_m, causing A_m to decline. With the now-depressed level of A_m, R_a is able to recover and reassemble the actomyosin network, which sets up the next cycle of oscillation. The duration of the actomyosin contraction depends on how long A_m persists with Baz. Higher Baz prolongs the contraction phase, as observed by David et al. (7).

It is interesting to note that the amplitude of the oscillation gradually declines in time for all proteins. The first few cycles have particularly large amplitudes. This is related to our model assumptions that initially all aPKC and Baz are stored in the circumference of the cell's apical surface and that the rate of recruitment to the medial domain is proportional to the entire stores of A_c and B_c (Eqs. 1 and 2). Thus, the first few large waves are incidental to the setup of the simulation and practically inconsequential. However, a more consequential feature is that the circumferential stores of aPKC and Baz are finite and decline in time as more of them translocate to the apicomedial domain to mediate the actomyosin dynamics. We will return to the temporal decline of the amplitudes when discussing the transition to the slow and fast phases.

Thus, the model explains the oscillatory behavior of the AS cells from the cell-autonomous kinetics of signaling proteins involved in DC. The question of whether cell oscillation arises from intracellular or intercellular mechanisms has been debated in the literature. Some mathematical models, including our model and that of Machado et al. (11), can produce oscillation from cell-autonomous mechanisms, whereas others rely on the mechanical coupling between neighbors (1,22). There is little doubt that the

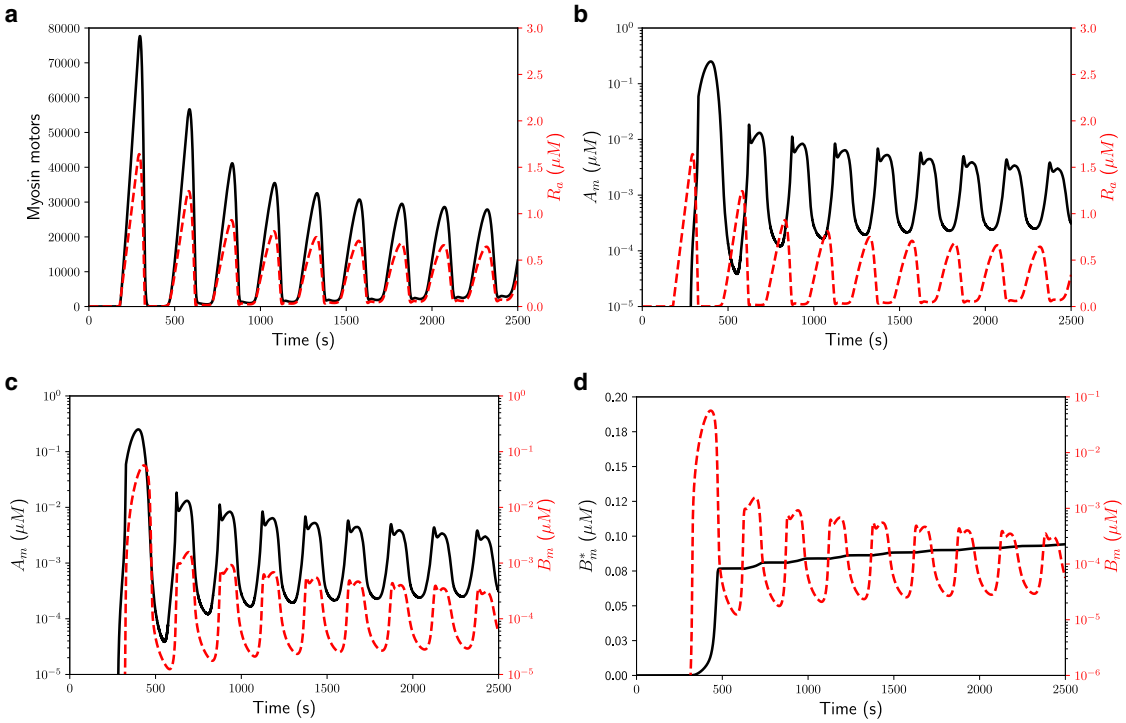

FIGURE 4 Evolution of various medial proteins in the representative cell during the early phase. (*a*) The number of myosin motors (*black*) and concentration of the actomyosin regulator R_a (*red dashed*). (*b*) R_a (*red dashed*) and its antagonizer aPKC A_m (*black*). (*c*) A_m (*black*) and Baz B_m (*red dashed*). (*d*) Baz cluster B_m^* (*black*) and B_m (*red dashed*). To see this figure in color, go online.

contractile phase of the oscillation is due to myosin motors inside each cell. It is the expansion phase that is in question. Experiments using holographic laser microsurgery (34) suggest that cell expansion is driven by intracellular forces and is thus cell autonomous. More recent data (12) paint a subtler picture in which a combination of autonomous and nonautonomous mechanisms drive cell expansion during AS oscillation. In our model, expansion occurs via passive elasticity of the cell, whose structural basis must be the actomyosin cortex. In this sense, our model is consistent with the cell-autonomous expansion noted by Hara et al. (12). But it does not discount an alternative pathway to oscillation through cell-cell coupling, which may coexist and cooperate with the cell-autonomous pathway in the real AS.

To sum up this subsection, our model is closely based on the observed intracellular kinetics of PAR proteins during DC (7,15) and their effects on actomyosin observed in *Drosophila* and other organisms (41,42). The possibility of aPKC phosphorylating Reg and complexing Baz results in a competition between the latter two and sets up negative feedback from aPKC onto actomyosin and from Baz onto aPKC. Thus, the oscillation arises in our model. By encoding the biological insights into a quantitative form, the model demonstrates a cell-autonomous mechanism for the oscillation.

Slow phase: ratcheting

The beginning of the slow phase is defined as the onset of net contraction of the AS tissue (3,4). In Fig. 2 *b*, we identify this as the instant $t = 2352$ s when the tissue area reaches a maximum before starting to decline. The end of the slow phase is marked by the cessation of cell area oscillation and a dramatic acceleration of AS contraction rate (4). Using the data of (4) as a reference and considering the variation among our model cells, we have determined the end of the slow phase at $t = 8046$ s, giving the slow phase a duration of 5694 s or roughly 95 min. Overall, the slow phase is characterized by a gradual intensification of net area contraction. Measured by its maximal area in each cycle, our representative cell of Fig. 2 *a* loses ~0.5% of area per cycle at the start up to 3% per cycle toward the end for a cumulative reduction of 20% during the slow phase. There is also a dampening of the amplitude of areal oscillation; it decreases from roughly 20% of the mean area to ~2% for the representative cell.

Our model captures the net decrease of cell area through an increasing average myosin level. This is evident from the temporal evolutions of both in the slow phase (Fig. 5 *a*). With each cell cycle, the minimal myosin level increases (*red arrow*); it stabilizes the cell cortex and prevents the cell from relaxing to its original area (*black arrow*). Tracing the biochemistry upstream, the increasing myosin level is the result of a gradually rising R_a, which in turn is due to its source q_R and a decline in the level of apicomedial aPKC A_m (Fig. 5 *b*). Because we have started with a finite reservoir of circumferential aPKC, A_c, the total amount of A_m is also finite. As more of it is sequestered by B_m^*, there is progressively less available A_m. As a result, R_a rises over each cycle.

A central concept in the current view of cell constriction is the internal ratchet (1,10,14,23). However, there is no convincing model or explanation of its underlying mechanism. The current hypothesis is that the cell cortex and internal actomyosin network stabilize themselves at the conclusion of every myosin pulse, thus preventing the cell area from returning to the previous value before the contraction (10,14,20). Then what stabilizes the actomyosin after each contractile pulse? Why is this behavior unique to the slow phase of DC but not present in the oscillatory early phase? In their DC model, Wang et al. (22) addressed this by prescribing an ad hoc "mechanical ratchet," reducing the resting length of each cell edge and spoke by a prescribed amount during the slow and late phases. Our model answers these questions on the basis of the biochemistry of the PAR proteins. During the early phase, there is still sufficient aPKC to antagonize the actomyosin regulator and allow the actomyosin network to

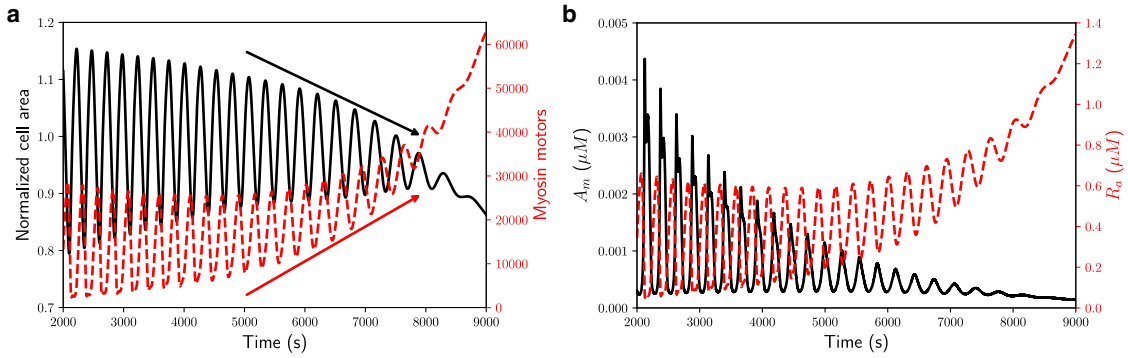

FIGURE 5 Evolution of various proteins in the representative cell during the slow phase. (*a*) Over each cycle of oscillation, an increase in myosin (*red dashed*) leads to constriction of the cell area (*black*), resulting in a ratchet-like effect. (*b*) The active Reg R_a (*red dashed*) rises over each cycle as the medial aPKC A_m (*black*) declines. To see this figure in color, go online.

disassemble. Consequently, the cell relaxes to its original area. The early phase comes to an end with the gradual exhaustion of apicomedial aPKC. In the slow phase, the declining level of aPKC is such that it is no longer able to completely suppress net myosin production in each cycle, resulting in a cumulative increase in the number of myosin motors with each successive cycle. This, our model suggests, is the molecular basis for the function of the actomyosin ratcheting.

The area of the entire AS tissue also shrinks gradually (Fig. 2 *b*), the contraction amounting to roughly 18% by the end of the slow phase. Experimentally, the beginning of the slow phase has been observed to coincide with the formation of the supracellular actin cable surrounding the AS tissue (3,4), suggesting a major role for the actin cable in AS contraction (1,3,4). Follow-up studies concluded, however, that the actin cable is not the main cause of closure (9,23,24) and contributes only a small fraction of the total area loss (22). Considering its relatively minor role, we have chosen to model the actin cable ad hoc at a coarser level than the intracellular dynamics (details in Supporting Materials and Methods, Section S1). Our model predictions confirm the insignificance of the actin cable to DC (details in Supporting Materials and Methods, Section S4; Video S2).

We close this subsection by noting two experimental features that the model fails to reproduce. First, Solon et al. (1) reported that the cessation of cell oscillation occurs first at the boundary with the epidermis and propagates inward toward the midline of the AS. In our model, all cells display roughly the same amplitudes of oscillation because the PAR protein dynamics are largely cell autonomous. Thus, the cessation of oscillation occurs randomly throughout the tissue, depending on the initial phase lag among the cells and their mechanical coupling. Second, in vivo, the amplitude of the oscillation dampens and its period shortens as the slow phase progresses (4). Our model captures the dampening of the oscillation due to the gradual buildup of apicomedial myosin but not the reduction in the period T. Our period actually lengthens, from ~260 s at the start to 350 s toward the end (Fig. 2 *a*). Evidently, our mathematical description of the PAR proteins misses some subtle mechanism that shortens the oscillation period in vivo. In the model of Machado et al. (11), AS cell oscillation arises from the cyclic actin turnover, and these authors were able to produce a shortening period by prescribing an actin turnover rate that increases in time. But at present, it is unclear what upstream mechanism could accelerate the actin turnover rate.

Fast phase: closure

The fast phase, as observed in vivo, introduces two new factors into the closure of the AS tissue. The first is zippering (25–27), which occurs when filopodia are extended from one epidermis to the other and exert a pulling force to move the two leading edges toward each other. We have chosen to exclude this factor from the model because it is nonessential for DC (9) and is largely independent of the AS contraction. The second is apoptosis and delamination of AS cells (3,8,28), which mainly occurs at the canthi during the onset of the zippering process and contributes to the speed of DC. We model this process by eliminating a cell when its area falls below a threshold area (1 μm^2) and all of its edges are shorter than 0.5 μm (Fig. S11). To maintain the integrity of the model tissue, we then collapse the outer nodes of the "apoptotic" cell onto the central node, a treatment motivated by in vivo experiments of Toyama et al. (28) and their Fig. 2, *a* and *b*. If eliminating a cell brings the opposing epidermis together, we consider this the fusion of the epidermis and subsequently fix the location of the central node. This mimics the restructuring process that occurs at the canthi in vivo (9).

Upon the onset of the fast phase, the AS cells stop oscillating and undergo persistent constriction while the tissue area drops precipitously (Fig. 2 *b*). The rapid loss of AS area lasts ~4000 s because the rate of contraction slows down. It takes roughly another 2000 s of slow contraction to reduce the AS area to below 5% of its initial value. This is considered "full closure" in our model, considering the lack of zippering. This duration of the fast phase is consistent with experimental observations (8,29). Video S1 gives an overall view of the whole process.

The evolving geometry of the AS is depicted in Fig. 6. At the start of the fast phase ($t = 8046$ s), the geometry of the AS tissue resembles that of a rounded rhombus (Fig. 6 *a*). As contraction becomes more intense, the outermost cells on the anterior-posterior axis are the first to become eligible for apoptosis (Fig. 6 *b*). Their elimination forms two canthi around $t = 10{,}100$ s. Once the canthi fix the length of the AS tissue, it narrows rapidly into a spindle shape (Fig. 6 *c*) that closely resembles the in vivo observation (9). In time, our AS tissue is able to shrink its area to below 5% of the initial value, producing a thin slit between the two epidermal tissues (Fig. 6 *d*). This is the final "fully closed" geometry. The closure is a robust prediction of our model that is attained with and without the actin cable (Fig. S7) and over wide ranges of the kinetic parameters (see a parametric study in Supporting Materials and Methods, Section S2).

What triggers the transition from the slow to the fast phase is the exhaustion of apicomedial aPKC. This is consistent with experimental observations of increased sequestration of aPKC by Baz in late DC (Fig. 5; (15)). Through the cycles of actomyosin assembly and disassembly of the early and slow phases, most of the circumferential aPKC (A_c) has translocated to the medial domain, and the medial aPKC (A_m) is gradually sequestered by B_m^*. Fig. 7 *a* shows the declining amplitude and mean of A_m in the early and slow phases, as each cycle receives less influx of aPKC from the circumferential A_c. Because B_m is

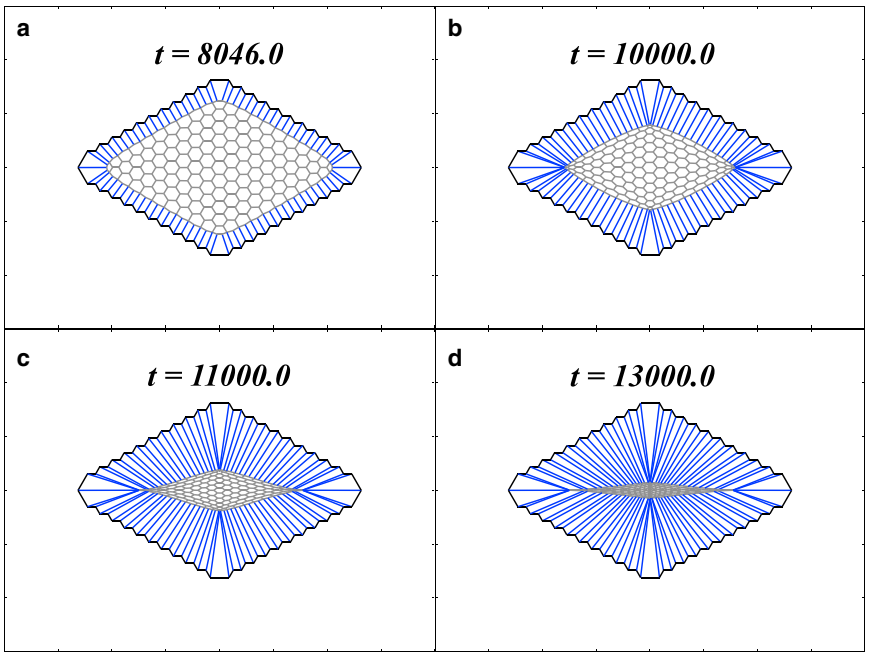

FIGURE 6 Contraction of the AS in the fast phase. (*a*) At the start of the fast phase $t = 8046$ s, the tissue boundary has been smoothed by the actin cable as compared to the initial configuration. (*b*) The AS shortly before the canthi form around $t = 10{,}100$ s. (*c*) After canthi formation, the AS narrows rapidly in the medial-lateral direction. (*d*) At $t = 13{,}000$ s, the tissue area has fallen below 5% of its initial value, and this is considered full closure in the context of our modeling. To see this figure in color, go online.

recruited by A_m to the apicomedial domain, it follows a similar trend of decline. By the end of the slow phase, A_m and B_m have more or less approached a steady state, as have the products AB and AR (Fig. 7 *b*). Henceforth, A_m and B_m have essentially dropped out of the negative feedback that antagonizes R_a and suppresses the assembly of myosin. This triggers the transition into the fast phase as the myosin pulsation gives way to a monotonic rise (Fig. 7 *c*), and the cell-area oscillation to persistent constriction. Note that the steady-state B_m concentration is

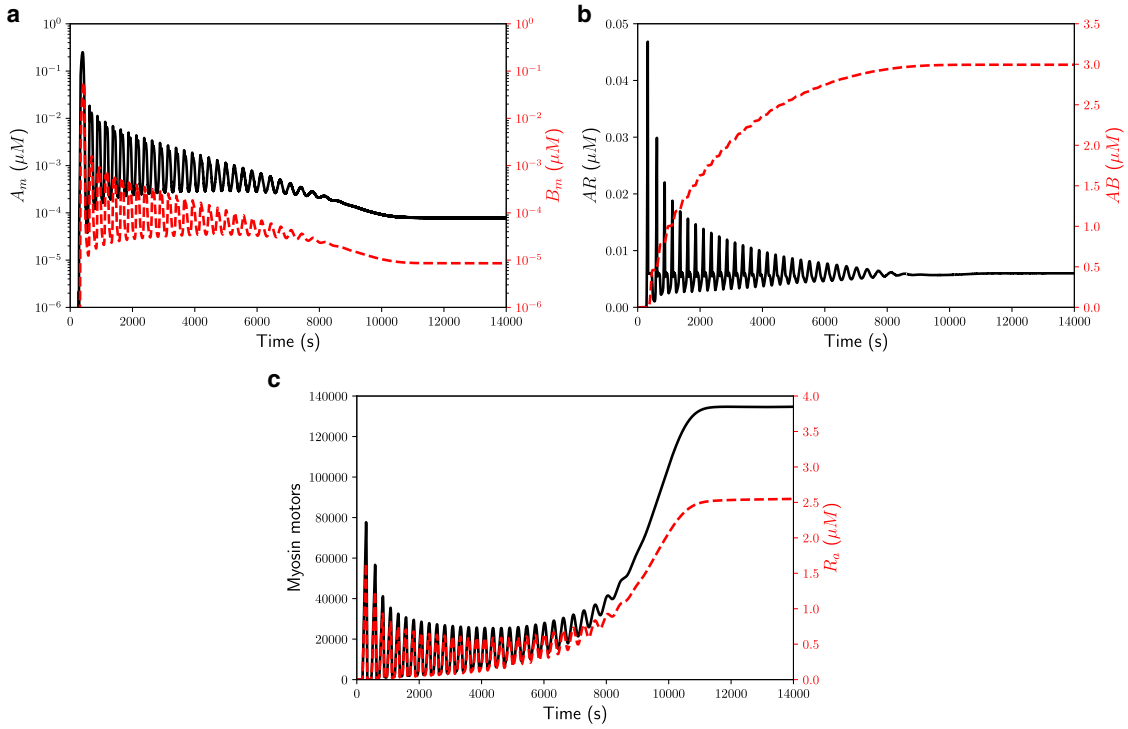

FIGURE 7 Dynamics of the key proteins in the representative cell explain the transition into the fast phase. (*a*) A_m (*black*) and B_m (*red dashed*) decline as medial aPKC is consumed by phosphorylation of Reg and Baz. (*b*) The products AR (*black*) and AB (*red dashed*) attain a steady state in time. (*c*) Oscillations in myosin (*black*) and R_a (*red dashed*) in the slow phase give way to monotonic growth in the fast phase. To see this figure in color, go online.

considerably lower than that of A_m. This observation is consistent with experimental observations of less Baz than Par-6 in the apicomedial complexes (15).

Interestingly, we find that the circumferential Baz store B_c has little effect on the onset of the fast phase. Although the entire circumferential store A_c is eventually recruited by Reg to the apicomedial region, the same is not true for B_c (Fig. S8). As A_m declines in the fast phase by way of Baz sequestration (Fig. 7 *a*), so does its ability to effectively recruit Baz from the periphery to the medial domain. Thus, the transport of B_c to B_m dies out, with only ~4% of B_c having reached the apicomedial domain. Such a low level of apicomedial Baz is sufficient to carry out its task of sequestering aPKC, partly because of our assumption of B_m^* not being saturated in its capability of sequestering aPKC (Eq. 8). Biologically, the rationale is that the Baz cluster B_m^* has multiple binding sites for aPKC and thus is not rendered ineffectual after forming the first complexes with aPKC (15,39,50,51). Nevertheless, the large initial store of B_c is necessary for the early and slow phase (Fig. S5 *a*). Our kinetics is such that the rate of Baz migration is proportional to B_c Eq. 4. Thus, the large B_c maintains a sufficient rate of B_m to suppress aPKC and allow the actomyosin to reassemble.

The experimental consensus is that in the fast phase the PAR-proteins progressively accumulate apicomedially and the actomyosin network becomes more persistent and pervasive throughout the AS tissue (15,26). These observations guided the construction of the mathematical model described in Eqs. 1, 2, 3, 4, 6, 7, 8, and 9 and are recapitulated by our simulation results. The strengthened actomyosin network dampens the AS cell oscillations and effects persistent constriction (1,4). Our model has predicted a natural transition from the slow to the fast phase and also captured its key features noted above. In this regard, it marks an advance beyond previous modeling, which has rarely dealt with the fast phase (1,11,34,35). An earlier model from our group (22), for example, was unable to predict the upsurge of apicomedial myosin in the fast phase. There was no chemical or mechanical cue to trigger the transition from oscillatory to nonoscillatory dynamics in the apicomedial myosin dynamics. In its stead, a mechanical ratchet was employed to produce rapid closure of the tissue by reducing the rest length of the edges and spokes in time.

DISCUSSION

The objective of this work is to integrate experimental findings of the molecular signaling pathways in *Drosophila* DC into a quantitative and predictive model. The model has two key components. One is a PAR protein regulatory circuit that has been suggested by recent observations (15,39,43–45). The other is a vertex-based cell mechanics model that is driven by myosin contraction. The myosin activation by a regulator downstream of the PAR-kinetics provides the linkage between the two. The model parameters have been evaluated based on available data, and the robustness of the results has been tested by varying these parameters. The main results of the study consist of the following:

1. The model predicts the oscillations in the apical area of AS cells in the early phase and provides an explanation for it from the cell-autonomous biochemistry of the PAR proteins.
2. The model predicts the internal ratchet that causes a gradual loss of cell area in the slow phase of DC and explains its molecular mechanism based on the same biochemistry.
3. The model predicts the cessation of cellular oscillation in the fast and final phase of DC as well as the rapid and persistent contraction of cell and tissue area, again from the biochemistry.

The model predictions are in reasonable agreement with experiments. For example, it reproduces the various timescales of the process, including the period of oscillation and the duration of the three phases; confirms the antiphase correlation among neighbors and the minor role of the supracellular actin cable; and recapitulates the temporal dynamics of the key proteins, especially the intensification of apicomedial myosin in the later stage of DC. Therefore, from a minimal regulatory circuit and cell mechanics, the model is able to capture most key features of the experimental observations in the early, slow, and fast phases as well as the transition among them. It provides a coherent framework that connects the tissue- and cell-level events to the intracellular transport and interaction of the PAR proteins. These are the main contributions of our work.

Of the factors contributing to DC, we have accounted for the intracellular contraction of actomyosin, the supracellular actin cable, the interaction with the surrounding epidermis, and the delamination of apoptotic cells. Zippering, an important mechanism during the final stage of closure, has been neglected completely. Of the factors included, the actomyosin contraction is modeled with the greatest care; it is the centerpiece of the model. The three other factors are modeled more ad hoc, using convenient mechanical and mathematical constructs. This is partly for lack of an understanding of the underlying mechanisms and partly for their secondary roles in the DC process. As more is learned about them, the new knowledge can be used to refine the modeling. The model predicts the oscillatory dynamics of the early phase from a cell-autonomous mechanism. This leaves aside, but by no means discounts or disproves, potential roles of cell-cell coupling. Mechanical coupling occurs through forces and deformation, as accounted for by earlier models (1,22). There may also be biochemical coupling, as evidenced by the intriguing phenomenon of an actomyosin pulse propagating between neighbors (7). This suggests potential pathways through cadherin-based mechaniobiology at cell junctions (52,53) or through mechanically gated ion channels (54).

Of necessity, the model makes simplifying assumptions about a complex biological process and omits some of its less important elements. A key assumption is a steady source for the actomyosin regulator R_a because this lies at the root of the ratcheting and rapid closure in the last two phases. The identity of this regulator has been discussed by several groups (15,17,40–42), and Rok appears as a highly plausible candidate among several hypothesized. An obvious task for future experiments is to identify the regulator unambiguously. The assumption of its source and continual supply is also testable in future experiments by examining its gene expression and medial protein levels in relation to upstream regulators and downstream contractile myosin networks. Besides, for lack of precise knowledge of the stoichiometry of aPKC sequestration by Baz clusters, we have assigned unsaturated binding capability to these clusters. An unrealistic consequence is the minimal relocalization of Baz from the circumference to the medial domain in comparison to in vivo observations (e.g., Fig. 2 of David et al. (15)). Future experiments should investigate the complex formation between aPKC and Baz and gather quantitative data on the stoichiometry.

The most glaring failure of the model is that it predicts a lengthening period for the AS cell oscillation during the slow phase with internal ratcheting, whereas in reality, the damping of the oscillation is accompanied by a shortening of the period (4). We can think of two potential causes for the discrepancy, one geometric and the other mechanical. As DC progresses, the shrinking cellular area should entail faster transport for the PAR proteins and potentially accelerate the downstream kinetics. This is unaccounted for in the model. Furthermore, experiments show that the tissue is under increasing tension during DC, and its mechanics changes from fluid-like to solid-like (15,26,35). The strengthening of the actomyosin and the rising tension have been captured by the model. However, this gradual rigidification does not translate to an increase in oscillation frequency, as one may expect based on mechanical intuition. The model determines the frequency of AS oscillation mostly from the kinetics of the PAR proteins and does not take adequate account of the rheological properties of the cells and tissue, including viscoelasticity (35). The various shortcomings of the model may motivate remedies and refinements in future work.

SUPPORTING MATERIAL

Supporting Materials and Methods, 11 figures, four tables, and two videos are available at http://www.biophysj.org/biophysj/supplemental/S0006-3495(18)31161-5.

AUTHOR CONTRIBUTIONS

T.J.C.H. and J.J.F. designed the research project. C.H.D. performed the numerical computations. All three authors contributed to the model formulation, data analysis, and the writing of the article.

ACKNOWLEDGMENTS

We acknowledge financial support by Natural Sciences and Engineering Research Council of Canada through Discovery Grant No. 05862 (to J.J.F.) and No. 05617 (to T.J.C.H.). We thank William Lou and Amir Mafi for their contribution to an earlier version of the model and Shane Hutson and Christoph Schmidt for discussions after the presentation of this work at the American Physical Society March Meeting in 2018.

SUPPORTING CITATIONS

Reference (55–61) appear in the Supporting Material.

REFERENCES

1. Solon, J., A. Kaya-Çopur, …, D. Brunner. 2009. Pulsed forces timed by a ratchet-like mechanism drive directed tissue movement during dorsal closure. *Cell.* 137:1331–1342.
2. Ma, X., H. E. Lynch, …, M. S. Hutson. 2009. Probing embryonic tissue mechanics with laser hole drilling. *Phys. Biol.* 6:036004.
3. Gorfinkiel, N., G. B. Blanchard, …, A. Martinez Arias. 2009. Mechanical control of global cell behaviour during dorsal closure in *Drosophila*. *Development.* 136:1889–1898.
4. Blanchard, G. B., S. Murugesu, …, N. Gorfinkiel. 2010. Cytoskeletal dynamics and supracellular organisation of cell shape fluctuations during dorsal closure. *Development.* 137:2743–2752.
5. Saravanan, S., C. Meghana, and M. Narasimha. 2013. Local, cell-nonautonomous feedback regulation of myosin dynamics patterns transitions in cell behavior: a role for tension and geometry? *Mol. Biol. Cell.* 24:2350–2361.
6. Kiehart, D. P., J. M. Crawford, …, G. S. Edwards. 2017. Cell sheet morphogenesis: dorsal closure in *Drosophila melanogaster* as a model system. *Annu. Rev. Cell Dev. Biol.* 33:169–202.
7. David, D. J., A. Tishkina, and T. J. Harris. 2010. The PAR complex regulates pulsed actomyosin contractions during amnioserosa apical constriction in *Drosophila*. *Development.* 137:1645–1655.
8. Sokolow, A., Y. Toyama, …, G. S. Edwards. 2012. Cell ingression and apical shape oscillations during dorsal closure in *Drosophila*. *Biophys. J.* 102:969–979.
9. Wells, A. R., R. S. Zou, …, D. P. Kiehart. 2014. Complete canthi removal reveals that forces from the amnioserosa alone are sufficient to drive dorsal closure in *Drosophila*. *Mol. Biol. Cell.* 25:3552–3568.
10. Martin, A. C., M. Kaschube, and E. F. Wieschaus. 2009. Pulsed contractions of an actin-myosin network drive apical constriction. *Nature.* 457:495–499.
11. Machado, P. F., G. B. Blanchard, …, N. Gorfinkiel. 2014. Cytoskeletal turnover and myosin contractility drive cell autonomous oscillations in a model of *Drosophila* dorsal closure. *Eur. Phys. J. Spec. Top.* 223:1391–1402.
12. Hara, Y., M. Shagirov, and Y. Toyama. 2016. Cell boundary elongation by non-autonomous contractility in cell oscillation. *Curr. Biol.* 26: 2388–2396.
13. Munjal, A., and T. Lecuit. 2014. Actomyosin networks and tissue morphogenesis. *Development.* 141:1789–1793.
14. Munjal, A., J. M. Philippe, …, T. Lecuit. 2015. A self-organized biomechanical network drives shape changes during tissue morphogenesis. *Nature.* 524:351–355.
15. David, D. J., Q. Wang, …, T. J. Harris. 2013. Bazooka inhibits aPKC to limit antagonism of actomyosin networks during amnioserosa apical constriction. *Development.* 140:4719–4729.
16. Azevedo, D., M. Antunes, …, A. Jacinto. 2011. DRhoGEF2 regulates cellular tension and cell pulsations in the Amnioserosa during *Drosophila* dorsal closure. *PLoS One.* 6:e23964.

17. Wang, H. R., Y. Zhang, …, J. L. Wrana. 2003. Regulation of cell polarity and protrusion formation by targeting RhoA for degradation. *Science.* 302:1775–1779.
18. Even-Faitelson, L., and S. Ravid. 2006. PAK1 and aPKCzeta regulate myosin II-B phosphorylation: a novel signaling pathway regulating filament assembly. *Mol. Biol. Cell.* 17:2869–2881.
19. Saias, L., J. Swoger, …, J. Solon. 2015. Decrease in cell volume generates contractile forces driving dorsal closure. *Dev. Cell.* 33:611–621.
20. Martin, A. C. 2010. Pulsation and stabilization: contractile forces that underlie morphogenesis. *Dev. Biol.* 341:114–125.
21. Kiehart, D. P., C. G. Galbraith, …, R. A. Montague. 2000. Multiple forces contribute to cell sheet morphogenesis for dorsal closure in *Drosophila*. *J. Cell Biol.* 149:471–490.
22. Wang, Q., J. J. Feng, and L. M. Pismen. 2012. A cell-level biomechanical model of *Drosophila* dorsal closure. *Biophys. J.* 103:2265–2274.
23. Pasakarnis, L., E. Frei, …, D. Brunner. 2016. Amnioserosa cell constriction but not epidermal actin cable tension autonomously drives dorsal closure. *Nat. Cell Biol.* 18:1161–1172.
24. Ducuing, A., and S. Vincent. 2016. The actin cable is dispensable in directing dorsal closure dynamics but neutralizes mechanical stress to prevent scarring in the *Drosophila* embryo. *Nat. Cell Biol.* 18:1149–1160.
25. Millard, T. H., and P. Martin. 2008. Dynamic analysis of filopodial interactions during the zippering phase of *Drosophila* dorsal closure. *Development.* 135:621–626.
26. Gorfinkiel, N., S. Schamberg, and G. B. Blanchard. 2011. Integrative approaches to morphogenesis: lessons from dorsal closure. *Genesis.* 49:522–533.
27. Lu, H., A. Sokolow, …, G. S. Edwards. 2015. Remodeling tissue interfaces and the thermodynamics of zipping during dorsal closure in *Drosophila*. *Biophys. J.* 109:2406–2417.
28. Toyama, Y., X. G. Peralta, …, G. S. Edwards. 2008. Apoptotic force and tissue dynamics during *Drosophila* embryogenesis. *Science.* 321:1683–1686.
29. Mateus, A. M., N. Gorfinkiel, …, A. Martinez Arias. 2011. Endocytic and recycling endosomes modulate cell shape changes and tissue behaviour during morphogenesis in *Drosophila*. *PLoS One.* 6:e18729.
30. Almeida, L., P. Bagnerini, …, F. Serman. 2011. A mathematical model for dorsal closure. *J. Theor. Biol.* 268:105–119.
31. Aristotelous, A. C., J. M. Crawford, …, S. Venakides. 2018. Mathematical models of dorsal closure. *Prog. Biophys. Mol. Biol.* 137:111–131.
32. Layton, A. T., Y. Toyama, …, S. Venakides. 2009. *Drosophila* morphogenesis: tissue force laws and the modeling of dorsal closure. *HFSP J.* 3:441–460.
33. Hutson, M. S., J. Veldhuis, …, G. W. Brodland. 2009. Combining laser microsurgery and finite element modeling to assess cell-level epithelial mechanics. *Biophys. J.* 97:3075–3085.
34. Jayasinghe, A. K., S. M. Crews, …, M. S. Hutson. 2013. Apical oscillations in amnioserosa cells: basolateral coupling and mechanical autonomy. *Biophys. J.* 105:255–265.
35. Machado, P. F., J. Duque, …, N. Gorfinkiel. 2015. Emergent material properties of developing epithelial tissues. *BMC Biol.* 13:98.
36. Gorfinkiel, N. 2013. Mechano-chemical coupling drives cell area oscillations during morphogenesis. *Biophys. J.* 104:1–3.
37. Harris, T. J. C., and J. J. Feng. 2014. Comment on Machado et al., "Cytoskeletal turnover and myosin contractility drive cell autonomous oscillations in a model of *Drosophila* dorsal closure. *Eur. Phys. J. Special Topics.* 223:1437–1439.
38. Hutson, M. S., Y. Tokutake, …, G. S. Edwards. 2003. Forces for morphogenesis investigated with laser microsurgery and quantitative modeling. *Science.* 300:145–149.
39. Renschler, F. A., S. R. Bruekner, …, S. Wiesner. 2018. Structural basis for the interaction between the cell polarity proteins Par3 and Par6. *Sci. Signal.* 11:eaam9899.
40. Zhang, H., and I. G. Macara. 2008. The PAR-6 polarity protein regulates dendritic spine morphogenesis through p190 RhoGAP and the Rho GTPase. *Dev. Cell.* 14:216–226.
41. Ishiuchi, T., and M. Takeichi. 2011. Willin and Par3 cooperatively regulate epithelial apical constriction through aPKC-mediated ROCK phosphorylation. *Nat. Cell Biol.* 13:860–866.
42. Röper, K. 2012. Anisotropy of Crumbs and aPKC drives myosin cable assembly during tube formation. *Dev. Cell.* 23:939–953.
43. Wang, S. C., T. Y. F. Low, …, F. Motegi. 2017. Cortical forces and CDC-42 control clustering of PAR proteins for *Caenorhabditis elegans* embryonic polarization. *Nat. Cell Biol.* 19:988–995.
44. Dickinson, D. J., F. Schwager, …, B. Goldstein. 2017. A single-cell biochemistry approach reveals PAR complex dynamics during cell polarization. *Dev. Cell.* 42:416–434.e11.
45. Rodriguez, J., F. Peglion, …, N. W. Goehring. 2017. aPKC cycles between functionally distinct PAR protein assemblies to drive cell polarity. *Dev. Cell.* 42:400–415.e9.
46. Graybill, C., B. Wee, …, K. E. Prehoda. 2012. Partitioning-defective protein 6 (Par-6) activates atypical protein kinase C (aPKC) by pseudosubstrate displacement. *J. Biol. Chem.* 287:21003–21011.
47. Tepass, U. 2012. The apical polarity protein network in *Drosophila* epithelial cells: regulation of polarity, junctions, morphogenesis, cell growth, and survival. *Annu. Rev. Cell Dev. Biol.* 28:655–685.
48. Zahedi, B., W. Shen, …, N. Harden. 2008. Leading edge-secreted Dpp cooperates with ACK-dependent signaling from the amnioserosa to regulate myosin levels during dorsal closure. *Dev. Dyn.* 237:2936–2946.
49. Harris, T. J. C. 2017. Protein clustering for cell polarity: Par-3 as a paradigm. *F1000Res.* 6:1620.
50. Morais-de-Sá, E., V. Mirouse, and D. St Johnston. 2010. aPKC phosphorylation of Bazooka defines the apical/lateral border in *Drosophila* epithelial cells. *Cell.* 141:509–523.
51. Wodarz, A., A. Ramrath, …, E. Knust. 2000. *Drosophila* atypical protein kinase C associates with Bazooka and controls polarity of epithelia and neuroblasts. *J. Cell Biol.* 150:1361–1374.
52. Hoffman, B. D., C. Grashoff, and M. A. Schwartz. 2011. Dynamic molecular processes mediate cellular mechanotransduction. *Nature.* 475:316–323.
53. Hoffman, B. D., and A. S. Yap. 2015. Towards a dynamic understanding of cadherin-based mechanobiology. *Trends Cell Biol.* 25:803–814.
54. Hunter, G. L., J. M. Crawford, …, D. P. Kiehart. 2014. Ion channels contribute to the regulation of cell sheet forces during *Drosophila* dorsal closure. *Development.* 141:325–334.
55. Forgacs, G., R. A. Foty, …, M. S. Steinberg. 1998. Viscoelastic properties of living embryonic tissues: a quantitative study. *Biophys. J.* 74:2227–2234.
56. Kovács, M., K. Thirumurugan, …, J. R. Sellers. 2007. Load-dependent mechanism of nonmuscle myosin 2. *Proc. Natl. Acad. Sci. USA.* 104:9994–9999.
57. Besser, A., and U. S. Schwarz. 2007. Coupling biochemistry and mechanics in cell adhesion: a model for inhomogeneous stress fiber contraction. *New J. Phys.* 9:425.
58. Fernandez-Gonzalez, R., Sde. M. Simoes, …, J. A. Zallen. 2009. Myosin II dynamics are regulated by tension in intercalating cells. *Dev. Cell.* 17:736–743.
59. Phillips, R., J. Kondev, …, H. Garcia. 2012. Physical Biology of the Cell. Garland Science, New York.
60. Milo, R., and R. Phillips. 2015. Cell Biology by the Numbers. Garland Science, New York.
61. Hayes, P., and J. Solon. 2017. *Drosophila* dorsal closure: an orchestra of forces to zip shut the embryo. *Mech. Dev.* 144:2–10.

Biophysical Journal, Volume *115*

Supplemental Information

Dynamics of PAR Proteins Explain the Oscillation and Ratcheting Mechanisms in Dorsal Closure

Clinton H. Durney, Tony J.C. Harris, and James J. Feng

Supporting Material for "Dynamics of PAR proteins explain the oscillation and ratcheting mechanisms in dorsal closure"

C.H. Durney[1], T.J.C. Harris[2], J.J. Feng[1,3]

[1] Department of Mathematics, University of British Columbia, Vancouver, British Columbia, Canada
[2] Department of Cell & Systems Biology, University of Toronto, Toronto, Ontario, Canada
[3] Department of Chemical and Biological Engineering, University of British Columbia, Vancouver, British Columbia, Canada

S1 Mechanical model

The structure of our model is such that the kinetics of the PAR proteins feed into the mechanics of the amnioserosa through the active form of the regulator R_a. Since R_a is defined for each cell while the apicomedial myosin is defined on the six spokes, we use a geometric factor h_{ij} to distribute R_a onto each of its spokes (1):

$$h_{ij} = \frac{\frac{1}{2}\text{area of } \triangle_{i,j-1,j} + \frac{1}{2}\text{area of } \triangle_{i,j,j+1}}{\text{area of cell}},$$

where the numerator is the average of the area of the two triangles on either side of the spoke ij. On each spoke, the number of active myosin motors varies according to R_a-induced attachment at rate k^+ and spontaneous detachment at rate k^-:

$$\frac{dm_{ij}}{dt} = k^+ R_a h_{ij} - k^- m_{ij}, \tag{S1}$$

where the myosin detachment is suppressed by tension, based on a well-established positive feedback loop (2, 3):

$$k^- = \begin{cases} c_1 e^{-c_2 f_{ij}}, & f_{ij} > 0 \\ c_1, & f_{ij} \leq 0 \end{cases} \tag{S2}$$

The mechanical framework is essentially the same as in the previous model of Wang et al. (1). The force on any given node i by adjacent node j is given by

$$f_{ij} = \mu(l_{ij} - l_0) + \beta m_{ij}, \tag{S3}$$

where μ is the elastic modulus, l_{ij} and l_0 are the current length and the rest length of the cell edge or spoke, β is the force per myosin motor and m_{ij} denotes the number of myosin currently attached to a spoke. The sign convention is such that a positive

0006-3495/08/09/2624/12 $2.00

f_{ij} indicates tension on the segment. There is always cortical myosin, of course. But since it plays no major role during DC, we have absorbed its contractile effect into the resting length l_0 of an edge. Thus, only the apicomedial myosin is accounted for explicitly, and $m_{ij} = 0$ on an edge. Tissue deformation is realized by the nodal motion governed by over-damped dynamics with a viscous friction factor η:

$$\eta \frac{d\boldsymbol{x}_i}{dt} = \boldsymbol{f}_i = \sum_j f_{ij} \frac{\boldsymbol{x}_j - \boldsymbol{x}_i}{|\boldsymbol{x}_j - \boldsymbol{x}_i|}, \tag{S4}$$

where the force on the i^{th} node $\boldsymbol{f}_i$ sums the forces f_{ij} on each segment connecting node i to an adjacent node j. Based on the characteristic velocity of cell contraction, we estimate, a posteriori, the Reynolds number of the cytoplasmic flow to be on the order of 10^{-8}. Thus, the assumption of over-damped motion is fully justified. At the start of the simulation, there is no apicomedial myosin, and the initial length of the edges and spokes is such that the tissue is under an homogeneous tension (4).

The surrounding epidermis resists the dorsal closure (5, 6), but a detailed treatment of this resistance entails an account for the mechanics and structural remodeling of the epidermis (7). For simplicity and following prior modeling (4, 8), we use elastic tension lines to connect the outermost nodes of the AS tissue to a stationary outer boundary (blue lines Fig. 1a of the main text). These tension lines have the same elastic modulus μ and resting length l_0 as the edges and spokes in the interior, and initially carry a force that equals to the initial amnioserosa tension plus an extra tension F_c, the latter to anticipate the contraction of the tissue upon onset of medial myosin.

The supracellular actin cable forms on the interface between the epidermis and the AS. As the actin cable only plays a secondary role in the closure event (1, 9–11), we have elected to model it *ad hoc* by adding additional myosin along the outline of the AS tissue, i.e. through the outermost nodes (magenta in Fig. 1a of the main text):

$$m(t) = \begin{cases} 0, & t < t_0 \\ M \frac{t - t_0}{t_1 - t_0}, & t_0 \le t \le t_1 \\ M, & t > t_1. \end{cases} \tag{S5}$$

The piecewise linear form is motivated by recent *in vivo* imaging that suggests that the actomyosin in the actin cable increases roughly linearly during DC, saturating around 120 min (12, 13). The maximum M is chosen to be comparable to the maximum apicomedial myosin level during the early and slow phases. Although we know little of the signaling pathways upstream of the formation of the actin cable, the accumulation of myosin is likely through similar pathways to that of the cortical myosin and should be expressed at similar levels. The parameters t_0 and t_1 were chosen to match the curve presented in Fig. 2B of Hayes and Solon (13). Finally, we neglect zippering forces in our model. Although zippering is essential to the final fusing of the epidermis, it functions only at the end of the closure, and does not interact with the earlier dynamics on which this work focuses.

Table S1: Values of the parameters used in the model and their sources where available.

Parameters			Values	Sources
Kinetic	aPKC migration	k_1	$0.00125\ \mu\mathrm{M}^{-1}\,\mathrm{s}^{-1}$	
	Baz migration	k_2	$0.00125\ \mu\mathrm{M}^{-1}\,\mathrm{s}^{-1}$	
	aPKC/Reg reaction	k_3	$2.5\ \mathrm{s}^{-1}$	
	aPKC/Reg unbinding	k_4	$75.0\ \mu\mathrm{M}^{-1}\,\mathrm{s}^{-1}$	
	Baz clustering	k_5	$5.0\ \mu\mathrm{M}^{-1}\,\mathrm{s}^{-1}$	
	Baz cluster dissociation	k_6	$0.001\ \mathrm{s}^{-1}$	
	aPKC sequesteration	k_7	$3.5\ \mu\mathrm{M}^{-1}\,\mathrm{s}^{-1}$	
	aPKC release	k_8	$0.00001\ \mathrm{s}^{-1}$	
	Reg production	q_R	$0.015\ \mu\mathrm{M}\,\mathrm{s}^{-1}$	
	aPKC transport delay	τ	$100\ \mathrm{s}$	
	myosin attachment rate	k^+	$10^4\ \mu\mathrm{M}^{-1}\,\mathrm{s}^{-1}$	
	myosin detachment rate	c_1	$0.25\ \mathrm{s}^{-1}$	(2)
	tension-factor for myosin detachment	c_2	$1.33 \times 10^{-2}\ \mathrm{nN}^{-1}$	
Mechanical	spoke elastic modulus	μ	$0.75\ \mathrm{nN}\,\mu\mathrm{m}^{-1}$	(4)
	spoke rest length	l_0	$5.0\ \mu\mathrm{m}$	(4)
	force per myosin motor	β	$10^{-3}\ \mathrm{nN/motor}$	(14)
	viscous friction factor	η	$100.0\ \mathrm{nN\,s}\,\mu\mathrm{m}^{-1}$	(15, 16)
	constant epidermal tension	F_c	$5.0\ \mathrm{nN}$	
Initial Condtion	aPKC (circumferential)	A_c	$3.0\ \mu\mathrm{M}$	(17)
	Baz (circumferential)	B_c	$3.0\ \mu\mathrm{M}$	(17)
	all other proteins		0	
	spoke length	l_{ij}	$7.6\ \mu\mathrm{m}$	(4, 12, 18–20)
Actin Cable	maximum number of myosin	M	30000	
	initial onset	t_0	$2700\ \mathrm{s}$	(12, 13)
	time of saturation	t_1	$9900\ \mathrm{s}$	(12, 13)

S2 Model parameters and sensitivity analysis

The model parameters are tabulated in Table S1 in four categories: kinetic parameters, mechanical parameters, initial conditions and parameters for the supracellular actin cable. The parameter values are estimated from the experimental literature where possible, and such sources are listed as well. If no reliable information is available, we have chosen values to produce desirable model predictions. To address such uncertainties in parameter evaluation, we have performed a sensitivity analysis by varying each of the uncertain parameters from its baseline value listed in the table and examining how the model prediction changes. The conclusion is that the qualitative features of the model predictions are robust and prevail over a reasonably wide range of parameters. Quantitatively, of course, the results do vary with each of the parameters with a different degree of sensitivity. In the following we present details of the sensitivity tests.

S2.1 Kinetic parameters

This subsection focuses on the key kinetic parameters k_1, k_2, …, k_8, q_R and τ. Parameters involved in the actin cable (see Eq. S5) will be discussed separately in Sec. S4 below. Starting with the baseline values of the kinetic parameters of Table S1, we vary each of these parameters to find an upper and lower bound outside of which at least one of the desirable features of

Table S2: The lower bounds for the kinetic parameters, given as multiplicative factors that, when multiplied by the baseline parameter values, yield the thresholds for each parameter.

Parameter	Baseline	Lower bound	Oscillations	Dampening	Ratchet	Fast Phase
k_1	0.00125	0.5	Yes	Yes	Yes	No[1]
k_2	0.00125	0.2	Yes	Yes	Yes	No[1]
k_3	2.5	0.1	Yes	No[2]	Yes	Yes
k_4	75	0.4	Yes	Yes	Yes	No[3]
k_5	5	0.05	Yes	Yes	Yes	No[3]
k_6	0.001	0 [4]	Yes	Yes	Yes	Yes
k_7	3.5	0.25	Yes	Yes	Yes	No[1]
k_8	0.00001	0	Yes	No[5]	Yes	Yes
q_R	0.15	0.75	Yes	Yes	Yes	No[1]
τ	100	0.4	Yes[6]	Yes	Yes	No[1]

[1] Delayed onset of the fast phase.
[2] Increasing amplitude.
[3] Premature onset of fast phase.
[4] $k_6 = 0$ yields nearly identical results to the baseline.
[5] No discernible dampening of oscillations before onset of fast phase.
[6] Period too short.

Table S3: The upper bounds for the kinetic parameters given as multiplicative factors.

Parameter	Baseline	Upper bound	Oscillations	Dampening	Ratchet	Fast Phase
k_1	0.00125	2.00	Yes	Yes	Yes	No[1]
k_2	0.00125	10.00	Yes	Yes	Yes	No[1]
k_3	2.5	100.00	Yes	Yes	Yes	No[2]
k_4	75	4.00	Yes	Yes	Yes	No[2]
k_5	5	300.00	Yes	Yes	Yes	No[2]
k_6	0.001	100.00	Yes	Yes	Yes	No[1]
k_7	3.5	15.00	Yes	Yes	Yes	No[1]
k_8	0.00001	2.00	Yes	Yes	Yes	No[2]
q_R	0.15	2.33	Yes	No[3]	Yes	No[1]
τ	100	2.00	Yes[4]	Yes	Yes	No[1]

[1] Premature onset of fast phase.
[2] Delayed onset of fast phase.
[3] No discernible dampening of oscillations before onset of fast phase.
[4] Period too long.

dorsal closure (DC) is lost. The choice of these "desirable features" is somewhat subjective, and we have chosen the following four: oscillations sustained for the duration of the Early Phase, dampening of the oscillations during the Slow Phase, an appreciable ratcheting effect in the Slow Phase, and timely onset of the Fast Phase. Tables S2 and S3 report the lower and upper bounds for each of the kinetic parameters, along with information on which of the four features is lost and how. The baseline values were chosen from the literature when available and for those that no sources exist, a value was chosen as to maximize the desirable features stated above. Note that the bounds are reported as multiplicative factors that, when multiplied by the baseline parameter values, yield the thresholds for each parameter.

To illustrate graphically how an essential feature is lost when a certain parameter goes beyond the thresholds in the tables, we plot in Figs. S1 and S2 several solutions over a range of values for k_1 (periphery-to-medial transport rate of aPKC) and q_R

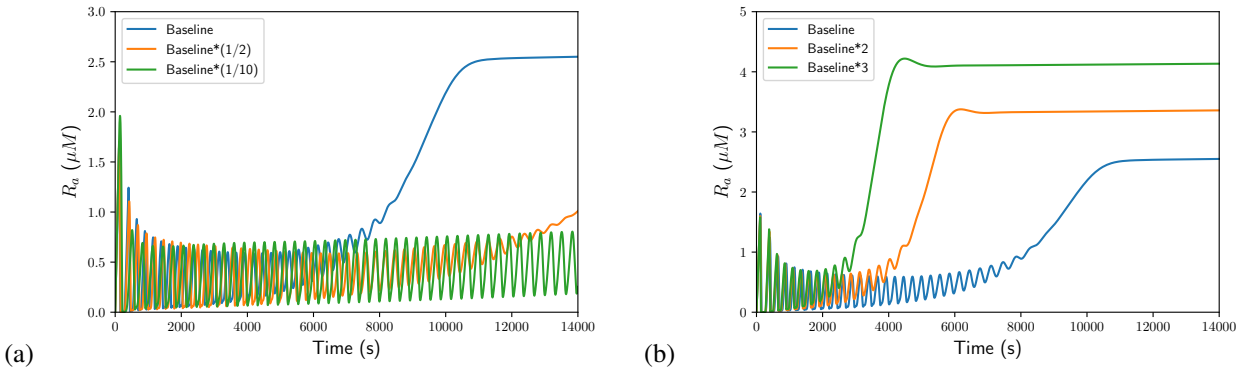

Figure S1: Effect of k_1 on R_a. (a) Decreasing k_1 causes oscillations to persist for longer, delaying and even losing entirely the ratchet and the transition to the fast phase. (b) Increasing k_1 shortens the early phase and causes premature closure.

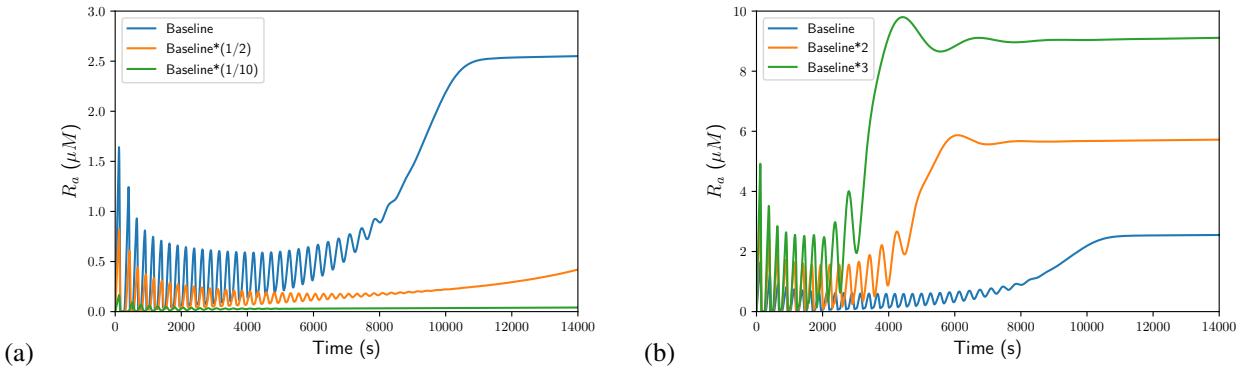

Figure S2: The effect of (a) decreasing q_R and (b) increasing q_R on the regulator R_a.

(source for actomyosin regulator), respectively. Similar sweeps have been carried out for the rest of the parameters and similar trends are seen. As noted in the main text, the qualitative features of DC are most sensitive to the dynamics of the active regulator R_a. It dictates the dynamics of apicomedial actomyosin and in turn the outcomes in cell oscillation and contraction. Thus, these figures plot R_a as the dependent variable.

Figure S1(a) shows that decreasing k_1 slows down the entire process. The oscillation of the early phase persists longer. Dampening of oscillation, ratcheting and the onset of the fast phase are delayed or even lost entirely. Consequently, such embryos would fail to close during the normal time frame of DC. Conversely, a large k_1 hastens the advent of ratcheting and the fast phase, at the expense of sustained oscillation of the early phase (Fig. S1b). One would expect premature closure for such embryos. Similar trends are observed for q_R in Fig. S2. Lower production of the regulator weakens the dynamics, reducing the amplitude of the R_a and myosin oscillations and eliminating ratcheting and persistent contraction. Such embryos will not contract much nor achieve closure. Elevated q_R, on the other hand, precipitates the ratcheting and the onset of the fast contraction and shortens the early phase. The dampening of oscillation in the slow phase also becomes indistinct. These embryos will close prematurely.

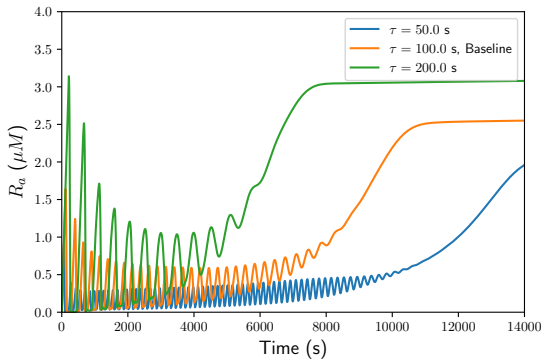

Figure S3: Effect of the delay parameter τ on R_a. A longer τ produces a longer period of oscillation.

In fact, similar trends appear through the entire parameter sweep, and we have identified a few general motifs. Across the entire parameter space $(k_1, \ldots, k_8, q_R, \tau)$, making the reactions slower preserves the oscillatory behavior and in most cases causes them to persist longer. This comes at the expense of the ratchet and onset of the fast phase. Thus, the early phase is prolonged while the slow and fast phases are delayed or even excluded from the duration of the simulation. Contrarily, increasing the kinetic parameters tends to disrupt cell oscillation, shorten or eliminate the early phase, and precipitate the slow and fast phase with a more pronounced ratcheting effect. Premature closure is the typical result.

Among all the parameters, the solution is most sensitive to the Reg production rate q_R, the aPKC migration rate k_1 and the delay in aPKC migration τ. These three exhibit the narrowest and most restrictive ranges for maintaining the four key features. Inspection of Eqs. (1–9) of the main text reveals that q_R directly affects the R_a production and appears nowhere else. Thus, its effect on R_a, which dictates features such as areal oscillation, ratcheting and fast-phase constriction, is unmitigated by other parameters. Similarly, k_1 and τ appear only in the transport of aPKC, another key factor in the model. The other kinetic parameters, in contrast, all appear in several equations. Their effects on R_a or A_m are modulated by additional parameters and thus less direct and stark. A good example is k_3. Even though it affects R_a in Eq. (5), k_3 also affects A_m and AR, with AR further influencing A_m through the k_4 term of Eq. (3). Consequently, the effect of k_3 on the model outcome is not as acute. Additionally, we found that the main control of the period of oscillation is the delay parameter τ. Increasing τ lengthens the period, whereas decreasing τ elevates the frequency of oscillations (Fig. S3). This result can be rationalized by noting that τ is the delay in aPKC transport from the circumference to the medial domain, and the medial aPKC, by recruiting Baz and phosphorylating Reg, is at the root of the actomyosin cycle. Finally, we note that reducing k_6 to 0 has little effect on the model predictions, and in particular maintains the four qualitative features defined in the above. This can be attributed to the already low rate of Baz cluster dissociation in comparison to cluster formation; cluster dissociation is dispensable in the model.

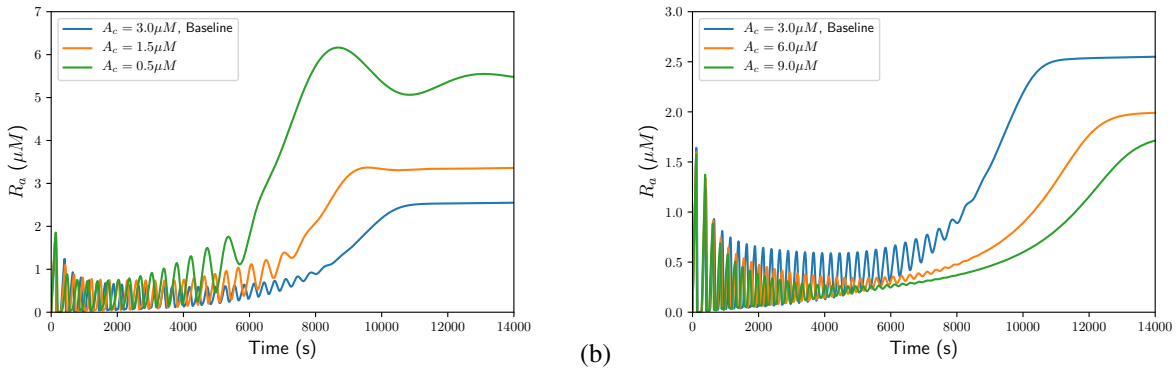

Figure S4: (a) Decreasing the initial circumferential store of aPKC, A_c, results in aPKC being exhausted prematurely and the embryo would transition into the fast phase too soon. (b) Increasing A_c results in decreased R_a concentrations.

S2.2 Initial conditions

As explained in the main paper, the ratcheting effect and onset of the fast phase are largely the result of depleting the circumferential aPKC store (A_c). We have also noted that only a small portion of the initial circumferential Baz (B_c) eventually participates in the medial actomyosin cycle. Therefore, we find it necessary to explore the dependence of the active Reg on the initial conditions of the circumferential PAR-proteins. The ranges of A_c and B_c that yield desirable behavior are summarized in Table S4.

Table S4: The upper and lower bounds for the initial conditions, given as multiplicative factors.

Parameter	Baseline	Bound	Oscillations	Dampening	Ratchet	Fast Phase
A_c (lower)	3.0	0.25	Yes	No[1]	Yes	Yes
A_c (upper)	3.0	2.00	Yes	Yes	Yes	No[2]
B_c (lower)	3.0	0.50	Yes	Yes	Yes	No[2]
B_c (upper)	3.0	5.00	Yes	Yes	Yes	No[3]

[1] No discernible dampening of oscillations before onset of fast phase.
[2] Delayed onset of fast phase.
[3] Premature onset of fast phase.

Unsurprisingly, we find that A_c and B_c have opposite effects on R_a. Lowering the initial A_c results in an increase in the overall R_a (Fig. S4a). Besides, the oscillatory early phase is shortened but has greater amplitude, whereas ratcheting and the slow phase become indistinct and quickly give way to a premature transition to the fast phase. The lower threshold can be put at $A_c = 0.75$ µM. Raising the initial A_c, on the other hand, tends to suppress the level of R_a (Fig. S4b). This is easily understood from Eqs. (3) and (5) of the main text. The upper bound is around $A_c = 6$ µM. Contrarily, decreasing the initial B_c results in a decrease of R_a over the course of DC (Fig. S5a). If B_c is too low, the embryo may stay in a state resembling the early phase for the duration of the entire simulation, with decreased amplitude of the cellular oscillations but very little ratcheting and no transition into the fast phase. At higher B_c, ratcheting and closure both happen earlier, with stronger actomyosin

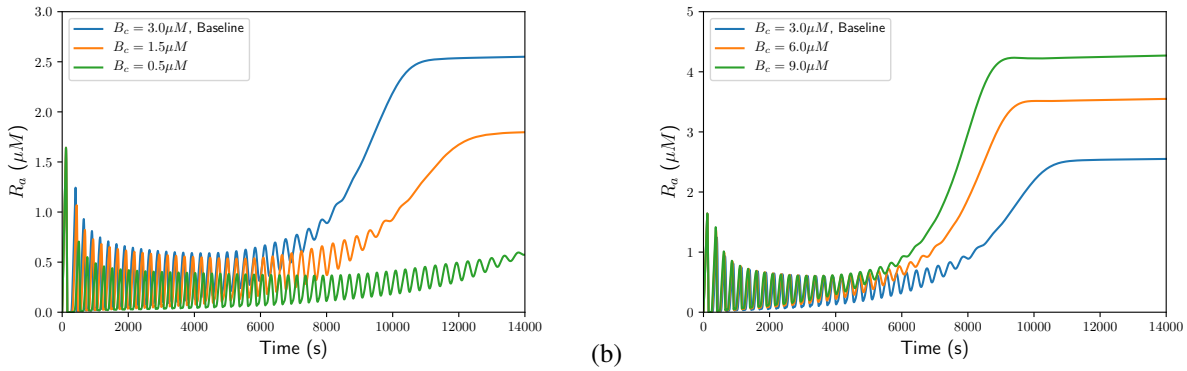

Figure S5: (a) Decreasing the initial circumferential store of Baz, B_c, results in a longer sustained oscillatory period and delayed onset of the fast phase. (b) Increasing B_c precipitates ratcheting and the transition to fast phase.

contraction (Fig. S5b). As noted in the main text, however, the model outcome is relatively insensitive to B_c. The lower and upper thresholds for B_c are 0.5 and 5 times the baseline value, respectively.

S3 Cross-correlations

During the early and slow phases, neighboring cells oscillate preferentially in antiphase. This is quantified by computing the cross-correlation of the areal change between neighbors, and averaging over the duration of the early and slow phases and over all 320 pairs of neighbors in the tissue. First, we calculate the instantaneous area A_i of any given cell i and its rolling mean over one period ($T \sim 260$ s):

$$\bar{A}_i(t) = \frac{1}{T}\int_{t-T/2}^{t+T/2} A_i(\tau)d\tau.$$

The difference $A_i(t) - \bar{A}_i(t)$ indicates the instantaneous state of expansion or contraction of the cell. We then calculate the cross-correlation of $A_i(t) - \bar{A}_i(t)$ with delay ΔT by two different methods. First, we use Python's Numpy.correlate function to calculate the cross-correlation between each pair of neighbors over the duration of the early and slow phase (from $t = 0$ to 8046 s) and average it over all 320 pairs of neighbors in the AS tissue. We have also calculated the cross-correlation by the following formula (4):

$$F_{cc}(\Delta T) = \frac{\sum_t (A_i(t) - \bar{A}_i)(A_j(t - \Delta T) - \bar{A}_j)}{\sqrt{\sum_t (A_i(t) - \bar{A}_i)^2 \sum_t (A_j(t - \Delta T) - \bar{A}_j)^2}}, \tag{S6}$$

where the summation is over the discrete time steps of our ODE solution within the early and slow phases. We then average $F_{cc}(\Delta T)$ over all cell-neighbor pairs. Both methods give the same result in Fig. S6(a). The negative peak at $\Delta T = 0$ demonstrates a preferentially antiphase correlation among neighbors. But the small magnitude (about -0.06) reflects the fact that cell neighbors exhibit both antiphase and in-phase correlation during their oscillation (4), and that on average the mechanical coupling has only a weak effect on cell oscillation.

We have also computed the cross-correlation between changes in a cell's area and its medial myosin, relative to their respective rolling mean values over a period T, averaged over all 121 cells in the AS tissue. Figure S6(b) shows that the area correlates negatively with the myosin, with a delay in time of about 27 s. This is consistent with experimental observations (18), the delay being due to viscous friction on nodal motion. Furthermore, the large magnitude of negative correlation (~ -0.92) indicates that the cell dynamics are primarily dictated by the internal myosin concentration of the cell. In comparison, neighbor-neighbor mechanical coupling plays a minor role in determining cell area oscillation (Fig. S6a).

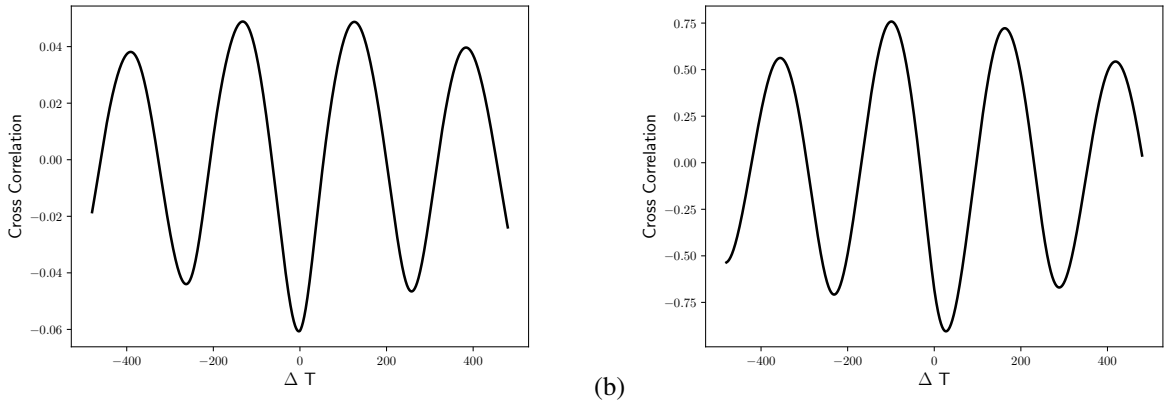

(a) (b)

Figure S6: (a) During the oscillation of the early and slow phases, neighboring cells exhibit a preferentially negative cross-correlation in area variation. The negative peak at $\Delta T = 0$ indicates antiphase oscillation between neighbors. (b) The cell area is strongly anti-correlated with the number of medial myosin motors. The negative peak is offset slightly from $\Delta T = 0$ because of the viscous friction that hinders nodal motion (Eq. S4).

S4 The role of the supracellular actin cable

To explore the significance of the actin cable to dorsal closure and our *ad hoc* treatment in Eq. (S5), we compare the model predictions with and without the actin cable (Fig. S7a). Turning on the actin cable causes a slight decrease in the tissue area subsequently, relative to the case without actin cable, but the effect is minimal (up to 2%). Visually, the actin cable tends to align the outermost cell edges so as to give the tissue a smoother leading edge. This is similar to the prediction of the earlier model of Wang et al. (1). Movie S2 depicts the entire closure process with the actin cable deactivated.

We have conducted further numerical tests on the timing of the actin cable. Figure S7(b) compares three runs with the actin cable activated at different times. An earlier onset does produce a smaller tissue area throughout, but the difference is minuscule. In particular, the instant at which the tissue area peaks before declining, which is taken to be the start of the slow phase, is not affected by the actin cable. Thus, in our model the actin cable is not the trigger for the start of the slow phase.

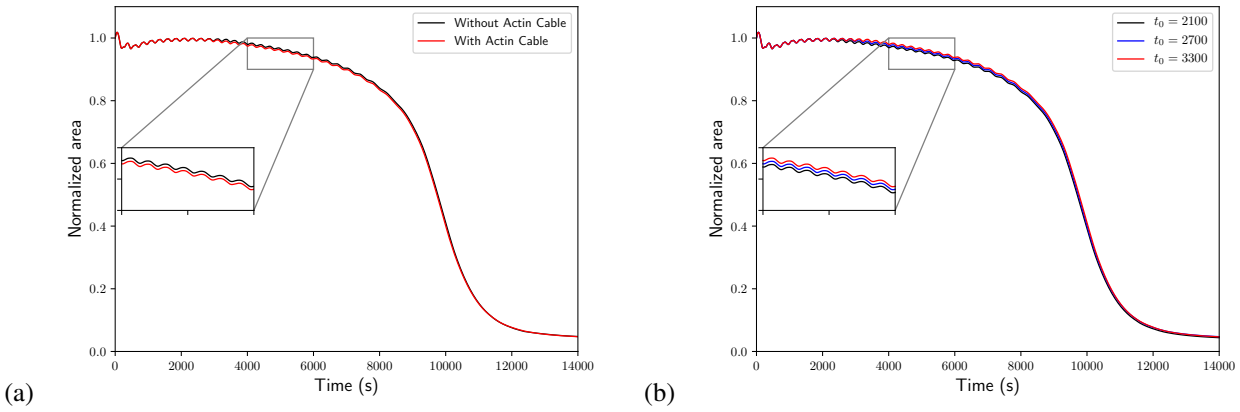

Figure S7: Effect of the actin cable on the temporal evolution of the tissue area. (a) Turning on the actin cable causes a slight decrease in the tissue area, in comparison to the case with no actin cable. (b) Activating the actin cable at different times has a minor effect on dorsal closure; an earlier activation decreases the tissue area slightly.

S5 Supplementary figures

The following figures are referred to by the main text.

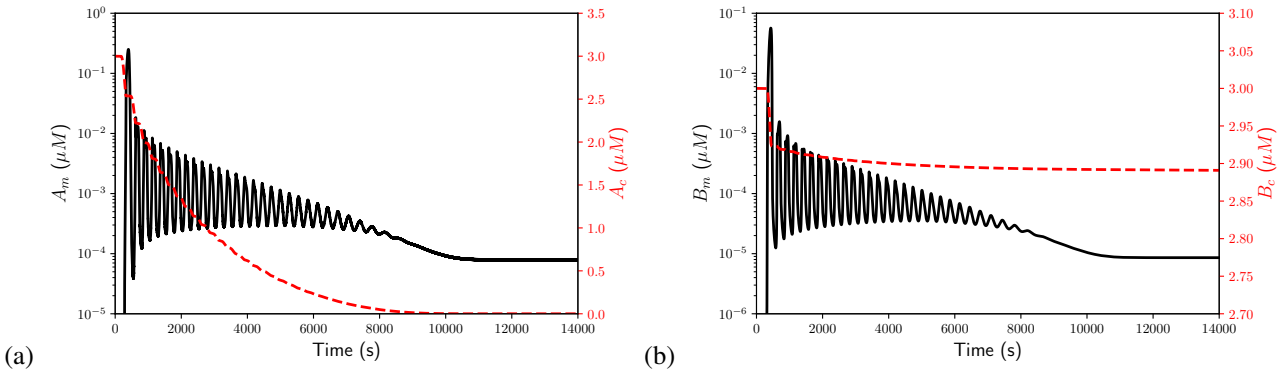

Figure S8: Transport of aPKC and Baz from the circumference to the medial domain. (a) Temporal evolution of A_m (black solid line) and A_c (red dashed line). (b) Temporal evolution of B_m (black solid line) and B_c (red dashed line).

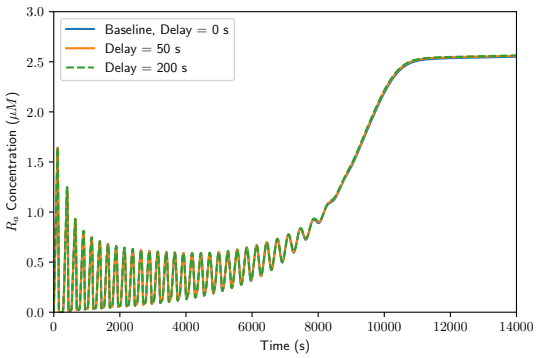

Figure S9: The model does not explicitly account for a time delay in the translocation of Baz from the periphery to the medial domain. Part of the reason is that the high capacity of apicomedial Baz clusters to sequester aPKC implies that only a small fraction of B_c is transported (see Fig. S8b). The three predictions shown here confirm that adding a Baz transport delay time into the model does not change its prediction significantly.

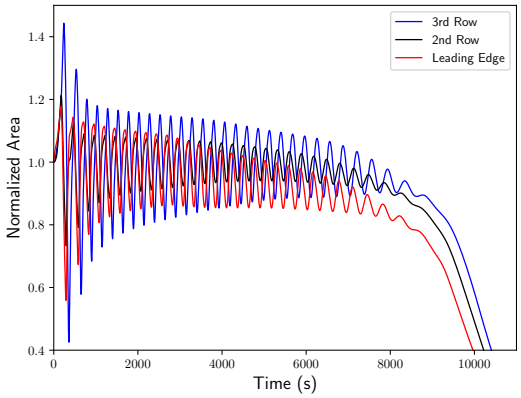

Figure S10: Behavior of a leading edge cell compared with that of cells in the next two rows towards the center. All three cells exhibit the same qualitative dynamics, and the cell oscillations persist for roughly the same length of time. The smaller amplitude of the leading edge cell is due to the blue tension lines representing the epidermis (Fig. 1).

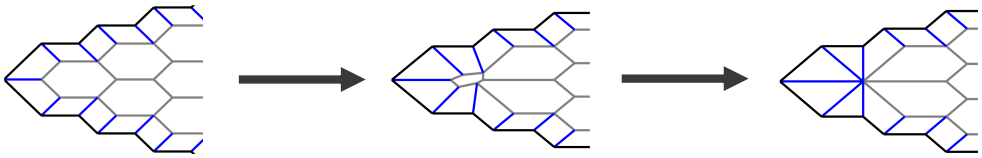

Figure S11: Schematic showing elimination of an "apoptotic" cell from the AS tissue. We model this process by eliminating a cell when its area falls below a threshold of 1 $\mu\mathrm{m}^2$ and all its edges are shorter than 0.5 $\mu\mathrm{m}$. To maintain the integrity of the model tissue, we collapse the outer nodes of the apoptotic cell onto the central node, a treatment motivated by *in vivo* experiments of Toyama et al. (21) and their Figure 2(a,b). If eliminating a cell brings the opposing epidermis together, as shown here, we consider this the fusion of the epidermis and subsequently fix the location of the central node. This mimics the *in vivo* restructuring process that occurs at the canthi (9). In our model prediction, only two cells are eliminated during the simulation and these are the left- and rightmost cells that form the canthi.

S6 Supplementary movies

Movie S1: Model simulation of the entire dorsal closure process using the baseline parameters of Table S1 of the online Supporting Material. The simulation exhibits the three distinct phases: early (0 – 2352 s), slow (2352 – 8046 s) and fast (8046 – 14000 s). The supracellular actin cable is activated at 2700 s. At the end the amnioserosa has shrunk to about 5% of its initial value.

Movie S2: A simulation with the same baseline parameters as Movie S1, but with the supracellular actin cable inactivated. Comparing the two movies, we see that the actin cable has only a cosmetic effect on the dorsal closure process; it smooths the tissue boundary by increasing tension in these edges.

References

1. Wang, Q., J. J. Feng, and L. M. Pismen, 2012. A cell-level biomechanical model of *Drosophila* dorsal closure. *Biophys. J.* 103:2265–2274.
2. Kovacs, M., K. Thirumurugan, P. J. Knight, and J. R. Sellers, 2007. Load-dependent mechanism of nonmuscle myosin 2. *Proc. Natl. Acad. Sci. U.S.A.* 104:9994–9999.
3. Fernandez-Gonzalez, R., S. de Matos Simões, J.-C. Röper, S. Eaton, and J. A. Zallen, 2009. Myosin II dynamics are regulated by tension in intercalating cells. *Dev. Cell* 17:736–743.
4. Solon, J., A. Kaya-Çopur, J. Colombelli, and D. Brunner, 2009. Pulsed forces timed by a ratchet-like mechanism drive directed tissue movement during dorsal closure. *Cell* 137:1331–1342.
5. Kiehart, D. P., C. G. Galbraith, K. A. Edwards, W. L. Rickoll, and R. A. Montague, 2000. Multiple forces contribute to cell sheet morphogenesis for dorsal closure in *Drosophila*. *J. Cell Biol.* 149:471–490.
6. Hutson, M. S., 2003. Forces for morphogenesis investigated with laser microsurgery and quantitative modeling. *Science* 300:145–149.
7. Gorfinkiel, N., S. Schamberg, and G. B. Blanchard, 2011. Integrative approaches to morphogenesis: Lessons from dorsal closure. *Genesis* 49:522–533.
8. Jayasinghe, A. K., S. M. Crews, D. N. Mashburn, and M. S. Hutson, 2013. Apical oscillations in amnioserosa cells: Basolateral coupling and mechanical autonomy. *Biophys. J.* 105:255–265.
9. Wells, A. R., R. S. Zou, U. S. Tulu, A. C. Sokolow, J. M. Crawford, G. S. Edwards, and D. P. Kiehart, 2014. Complete canthi removal reveals that forces from the amnioserosa alone are sufficient to drive dorsal closure in *Drosophila*. *Mol. Biol. Cell* 25:3552–68.
10. Ducuing, A., and S. Vincent, 2016. The actin cable is dispensable in directing dorsal closure dynamics but neutralizes mechanical stress to prevent scarring in the *Drosophila* embryo. *Nat. Cell Biol.* 18:1149–1160.
11. Pasakarnis, L., E. Frei, E. Caussinus, M. Affolter, and D. Brunner, 2016. Amnioserosa cell constriction but not epidermal actin cable tension autonomously drives dorsal closure. *Nat. Cell Biol.* 18:1161–1172.
12. Saias, L., J. Swoger, A. D'Angelo, P. Hayes, J. Colombelli, J. Sharpe, G. Salbreux, and J. Solon, 2015. Decrease in cell volume generates contractile forces driving dorsal closure. *Dev. Cell* 33:611–621.
13. Hayes, P., and J. Solon, 2017. *Drosophila* dorsal closure: An orchestra of forces to zip shut the embryo. *Mech. Develop.* 144:2–10.

14. Phillips, R., J. Kondev, J. Theriot, and H. Garcia, 2012. Physical Biology of the Cell. Garland Science.

15. Forgacs, G., R. A. Foty, Y. Shafrir, and M. S. Steinberg, 1998. Viscoelastic properties of living embryonic tissues: A quantitative study. *Biophys. J.* 74:2227–2234.

16. Besser, A., and U. S. Schwarz, 2007. Coupling biochemistry and mechanics in cell adhesion: A model for inhomogeneous stress fiber contraction. *New J. Phys.* 9:425.

17. Milo, R., and R. Phillips, 2015. Cell Biology by the Numbers. Garland Science.

18. Blanchard, G. B., S. Murugesu, R. J. Adams, A. Martinez-Arias, and N. Gorfinkiel, 2010. Cytoskeletal dynamics and supracellular organisation of cell shape fluctuations during dorsal closure. *Development* 137:2743–2752.

19. Gorfinkiel, N., G. B. Blanchard, R. J. Adams, and A. Martinez Arias, 2009. Mechanical control of global cell behaviour during dorsal closure in *Drosophila. Development* 136:1889–1898.

20. Machado, P. F., J. Duque, J. Étienne, A. Martinez-Arias, G. B. Blanchard, and N. Gorfinkiel, 2015. Emergent material properties of developing epithelial tissues. *BMC Biol.* 13:98.

21. Toyama, Y., X. G. Peralta, A. R. Wells, D. P. Kiehart, and G. S. Edwards, 2008. Apoptotic force and tissue dynamics during *Drosophila* embryogenesis. *Science* 321:1683–1686.